University of Strathclyde

Department of Physics, SUPA

The Use Of Infrared Spectroscopy To Examine Model Poly-Peptide And Enzyme Systems

Amy C. Welsh

Master of Philosophy

2011

This thesis is the result of the author's original research. It has been composed by the author and has not been previously submitted for examination which has led to the award of a degree.

Signed:

Amy Cara Welsh

Date: April 2012

Acknowledgments

I would like to begin by thanking my supervisor, Neil Hunt for his guidance throughout my research. Also to my colleagues in the UCP group, especially Spyridon Kaziannis and Stefano Santabarbara for help and advice during their time in the group. Many thanks to Bob Dawson and John Revie for their technical expertise.

To my friends in the Department of Physics and beyond, I am thankful to have met you. We have shared many laughs and I hope we will continue to.

I dedicate this thesis to my family, without whom I would not be who or where I am today. Thank you.

Contents

Abstract

Infrared spectroscopy is used here for the investigation of biomolecular interactions leading to changes in secondary structure conformations. These changes are observed in the Amide I band region of an Infrared spectrum where certain conformations have their own spectral signature.

The first type of interaction considered is that of self-assembling peptides. These systems have various applications ranging from biosensing to acting as a template for nano-wires. Such reactions display an equilibrium which can be described by the Gibbs Free Energy. These reactions provide many dynamics which can be easily observed with Infrared spectroscopic techniques.

Photo-initiated reactions are also considered, where a photoacid is used to activate reactions in model poly-peptide and enzyme systems. A helix-to-coil transition can be triggered by changing the pH of the solution. When dissolved in a photoacid, this transition is triggered when exposing the solution to ultraviolet light.

The photoacid is also used to protonate a model hydrogenase system to aid in the production molecular hydrogen. The model system is similar to the active site of complex enzyme systems. Using this model system removes the complication associated with the surrounding protein of such enzyme systems which protects the active site.

Chapter 1: Introduction

The understanding of the structure and function of biomolecules has become a popular topic in recent years and the motivation to understand biomolecular interactions has been driven by the fact that biological function and activity is related to biomolecular structure[1-3]. Dynamics of biomolecular interactions are important because it leads to an understanding of the biomolecule and reactions it undergoes[4-7]. The dynamics of protein interaction has been studied via temperature dependence[8,9] as well as pH titration[10-12].

There are many techniques which can be used to analyse biomolecules, more notably, nuclear magnetic resonance (NMR) spectroscopy[13], electron paramagnetic resonance[14,15] (EPR), circular dichroism[12,16-18] (CD), X-ray crystallography[19,20], ultraviolet and visible (UV/Vis) spectroscopy[21] and infrared (IR) spectroscopy. NMR spectroscopy uses the magnetic properties of a nucleus to determine information on the number and type of chemical constituents in a molecule. This technique is limited by time resolution and so is not ideal for determining kinetics in molecular systems[22]. EPR works on the principal that the chemical species it studies has one or more unpaired electrons. It is similar to NMR, however the electron spins are excited rather than that of atomic nuclei. EPR is not as widely used since most stable molecules have all paired electrons. Some molecules exhibit a property which means they do not have molecular symmetry and cannot be mirrored on itself, this property is known as chirality. The interaction of chiral molecules with polarised light is recorded using CD. The presence of a central carbon atom in a molecule often means the molecule is chiral. The angle at which residues are arranged in a peptide chain is dependent on chirality, which in turn determines the structure assumed by the peptide. This technique however, provides less information on a molecule than NMR or X-ray crystallography. Also, analysis of CD spectra can prove difficult due to artefacts caused by light scattering[22] which lead to misinterpretation of data. X-ray crystallography uses the scattering of X-rays from electrons and needs crystalline solids – crystals. The structure cannot be determined using X-ray crystallography if an organic compound is liquid, or is solid but doesn't form crystals[23]. Although time consuming, this method is useful in the determination of complicated structures. In IR spectroscopy, absorptions occur when electromagnetic waves interact with molecular vibrations.

Raman is a technique which is comparable to IR because it also depends on the vibrations of molecules. Raman does not require a change in dipole moment but does involve a change in polarisability. Raman is due to the scattering of light by a vibrating molecule whilst IR is the result of absorption of light in the vibrating molecule. Water can be used in Raman experiments but absorbs strongly in the Amide I region of IR spectra and so D_2O is often used in IR. The costs involved are relatively small for IR in comparison to Raman. Table 1.1 shows the resolution that can be achieved in various spectroscopic techniques used to study biomolecular reactions.

Technique	Steady State NMR[24]	2D NMR[24]	Ultrafast Transient Absorption[25]	Raman[26]	fs-stimulated Raman[27,28]
Time Resolution (s)	$10^{-12} – 10^{-3}$	$10^{0} – 10^{+3}$	100×10^{-15}	$10^{-9} – 10^{+3}$	$25 - 50 \times 10^{-15}$

Table 1.1: Spectroscopic Techniques and temporal resolutions.

In IR the normal mode vibrations correspond to the excitation from the ground state to the first excited state. Harmonic overtone bands relate to theoretically forbidden transitions where weak absorptions are found in IR spectra at approximately double the wavenumber of the 'normal' or 'fundamental' mode. These absorptions may be related to Fermi resonances when a mode is the sum of two frequencies and becomes separated on the frequency axis. This is caused by a shift of energy and intensity of an absorption band. Infrared spectroscopy can be used to determine structures of proteins and can also provide dynamics of interactions, making it a logical choice for studying biomolecular interactions. IR spectroscopy can give information on molecular structure and can provide information on the number of molecules present by considering the Beer-Lambert Law, Equation 2.1, via the absorption coefficient which has the SI unit m^2mol^{-1} i.e volume per mole.

The aim of this project is to understand the dynamics of biomolecular interactions via the use of Infrared spectroscopy. The project will focus on dynamics in various reactions and establishing the time dependence involved in the course of the reactions. The understanding of these reactions is important because the folding of proteins is related to their biological activity[29]. The functional site of a protein can be protected from contaminants by itself as it folds into a domain structure. Different IR spectroscopic methods are used depending on the speed of the interactions in question. Protein dynamics occur on a range of time scales[30] which can be observed using IR spectroscopy techniques. Time-resolved fourier transform infrared (FTIR) methods can be utilized to observe slow reactions, i.e. on a millisecond scale, like aggregation kinetics or the use of enzymes to catalyse the oxidation of organic compounds[31]. Faster reactions, ranging from domain folding ($\sim 10^{-6}$s) to chain diffusion, nucleation and folding of secondary structure ($\sim 10^{-9}$-10^{-6}s) or small fluctuations of side chains, torsions and hydrogen bonds ($\sim 10^{-13}$-10^{-11}s) can be observed using IR spectroscopy. Time-resolved IR methods have been employed for the study of the active site of heme proteins[32], which occur on a pico-second time scale. The Amide I region is easily observed with the use of IR spectroscopy. Model molecular systems illustrating the self-assembly of peptides are considered, as well as systems which undergo structural changes due to a photo-trigger.

This report will focus on FTIR and time resolved infrared (TRIR) spectroscopy. A recurring theme through-out the report is the initiation of reactions. In Chapter 3, a self-assembling peptide is considered since it features molecular interactions which can be easily observed using IR spectroscopy. Chapter 4 covers photo-initiated reactions i.e. the use of a photoacid to instigate the reactions which in one project, sees the conversion of the secondary structure of a model poly-peptide by altering the pH of the solution. Also discussed is the use of the same photoacid to protonate a hydrogenase enzyme system to aid in the production of molecular hydrogen. The photoacid was studied with both steady state FTIR and TRIR spectroscopy due to the fast processes observed.

The self-assembly of peptides has been studied for many years[33-40], discussing the building blocks of the reactions and observing them using techniques like atomic force microscopy (AFM), transmission electron microscopy (TEM)[35,40] as well as circular dichroism (CD), scanning electron microscopy (SEM)[38] and NMR spectroscopy[39]. Few studies have considered IR spectroscopy, but 2DIR spectroscopic analysis have been reported recently[22,41]. These systems are of interest because when peptides aggregate, they can lead to the development of neuro-degenerative diseases[42,43]. If the self-assembly process can be understood, it may be possible to prevent aggregation. Self-assembly is like protein aggregation with no outside contribution, such as a temperature or pH jump. In this report, time-dependent FTIR and UV-Vis studies were carried out on a self-assembly system to observe the development of Amide I content, i.e. secondary structure. The time dependence allowed the speed of these developments to be examined.

The use of IR spectroscopy to observe photo-chemical reactions has been well reported[44-46]. The photo-chemistry of o-nitrobenzaldehyde is not a new topic[47], as with pH induced protein folding[48]. FTIR and TRIR spectroscopy have been employed here to observe how the photoacid undergoes the transformation to acid after being triggered using a UV light source. The information gained from these experiments allowed time scales to be determined for the reaction, allowing the mechanisms to be fully understood before applying the use of the photoacid in photo-triggered reactions; a pH induced secondary structure change and protonation of a model hydrogenase enzyme system. The helix-to-coil conversion of poly-L-Lysine has been observed before[30], but not using a photo-trigger to change the pH as discussed here. Again, hydrogenases have been studied previously using 2DIR[49] without the aid of a photoacid to initiate the reaction. They have also been studied via a stopped-flow technique and time resolved IR spectroscopy[50,51]. Hydrogenase systems are interesting because of their application to energy transduction[50].

Chapter 2: Experimental Set-Up

Infrared Spectroscopy

Infrared spectroscopy is the study of molecular vibrations, more specifically, molecular bond vibrations. It detects the stretching and bending of bonds rather than properties of the atoms themselves[23]. It has been used for many years to examine biomolecules[29,52-54] and is a valuable tool for the understanding of molecular interactions. Biomolecular structures and their dynamics within reactions are studied here using IR spectroscopy, which is sensitive to protein conformation, making it ideal for probing such dynamics.

The use of IR Spectroscopy provides an insight into the amount of energy absorbed by the molecular vibrations. Most vibrations are within the Mid-IR region. This is because the vibrations are excited at these wavelengths. An FTIR spectrum measures the frequency of vibrations and is measured in wavenumbers, cm^{-1}. The spectrum is split into sections, or bands, along the frequency axis: Amide I, II, III, and A band regions. Figure 2.1 shows an amino acid from a protein labelled with stretching vibrations found in the Amide bands.

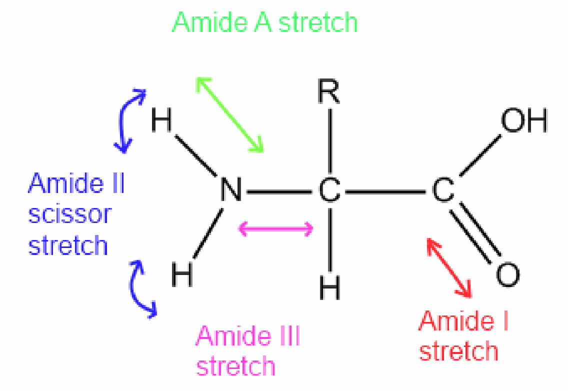

Figure 2.1: Simple amino acid in a protein labelled with amide vibrations.

These bands will be described later in this chapter. Quantum theory states that spectral lines are understood as the difference between vibrational energy levels. Energy is proportional to frequency, or wavenumber. C=O vibrations in amino acids, proteins and peptides are measured between $1600-1700cm^{-1}$, and are known as the Amide I band region. Vibrations in a molecule which have a centre of symmetry that are Raman active are IR inactive, and vice-versa. This is known as the Mutual Exclusion Principle. In some molecules, there may be bands which are IR active, and others which are Raman active, since there may be different symmetries in the molecule.

Spectroscopy of Proteins

Proteins are constructed from a sequence of amino acids. Amino acids consist of a central Carbon atom, connected to an amino group (NH_2), a carboxyl group (COOH), a hydrogen and a side chain (R group). The amino acids are linked via –CONH-, a peptide link, which is formed from the loss of water (OH from the carboxyl group) and H from the amino group, as seen in Figure 2.2.

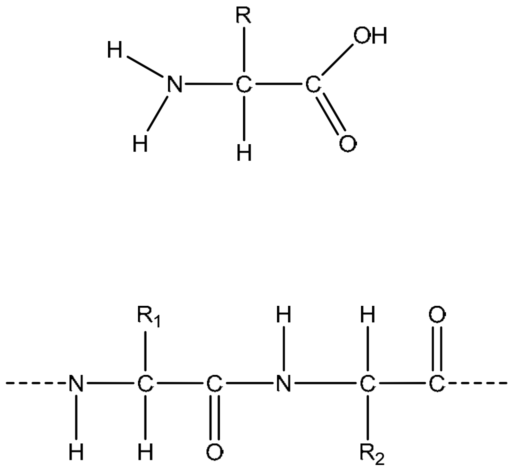

Figure 2.2: Amino acid, top. Two amino acids joined with a peptide link, bottom.

Protein structure can be split into four categories; primary, secondary, tertiary and quaternary structures. The primary structure describes the arrangement of the amino acids along the polypeptide chain. There are twenty naturally occurring amino acids. The three-dimensional form of the polypeptide chain is described by the secondary structure. The tertiary structure of peptide chains describes the three-dimensional arrangement of the secondary structure motifs within the protein domain. The quaternary structure contains several subunits of tertiary structures which aggregate together to form the final protein. Only proteins containing at least two amino acid chains have quaternary structure[55]. The secondary structure is defined by the pattern of hydrogen bonding to form structural motifs.

Hydrogen bonds are described as an attractive interaction between two atoms; hydrogen is bonded to one atom which is electronegative, and so shares its electron, making it slightly positive. It is a type of dipole-dipole attraction between molecules. It results from an attractive force between a hydrogen atom covalently bonded to a highly electronegative atom, like oxygen, nitrogen and fluorine or anionic species. The electronegativity is a measure of the power an atom has to attract electrons to itself when part of a compound. For an alpha-helix configuration, Figure 2.3, there is an H-bond between the backbone N-H and backbone C=O of the amino acid situated four residues earlier. A "residue" refers to an amino acid like that shown in Figure 2.2.

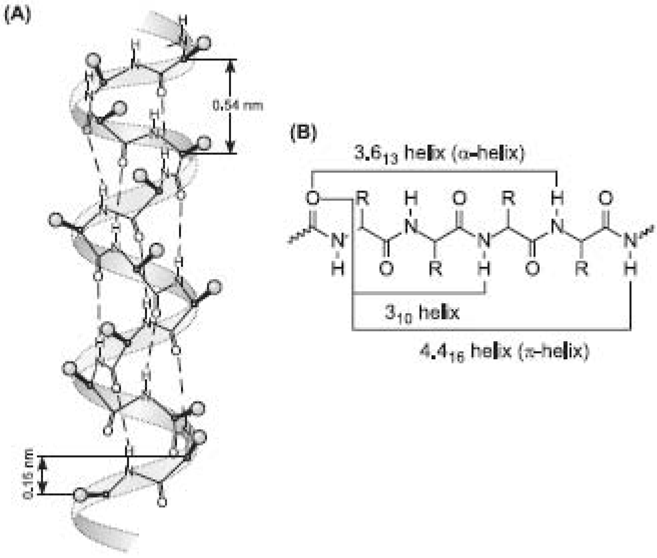

Figure 2.3: (A) Alpha-helix structure, (B) the H-bond pattern[56].

The alpha-helix is one of the configurations that make up the secondary structure of a protein. Another conformation is known as the beta-sheet. Beta-sheets are formed through H-bonding between two extended polypeptide chains. They can be either parallel or anti-parallel, as shown in Figure 2.4. R groups point above and below the plain of the sheet. In an anti-parallel beta-sheet, each N-H bond in one chain is aligned with a C-O bond from another chain. In parallel beta-sheets, the N-

H bonds are aligned to other N-H bonds, similarly for C-O bonds. A random coil is a length of peptide chain that is not in a definitive pattern like an alpha-helix or beta-sheet. The structure a peptide chain assumes is dependent on the rotation of amino acids on the chain around a bond.

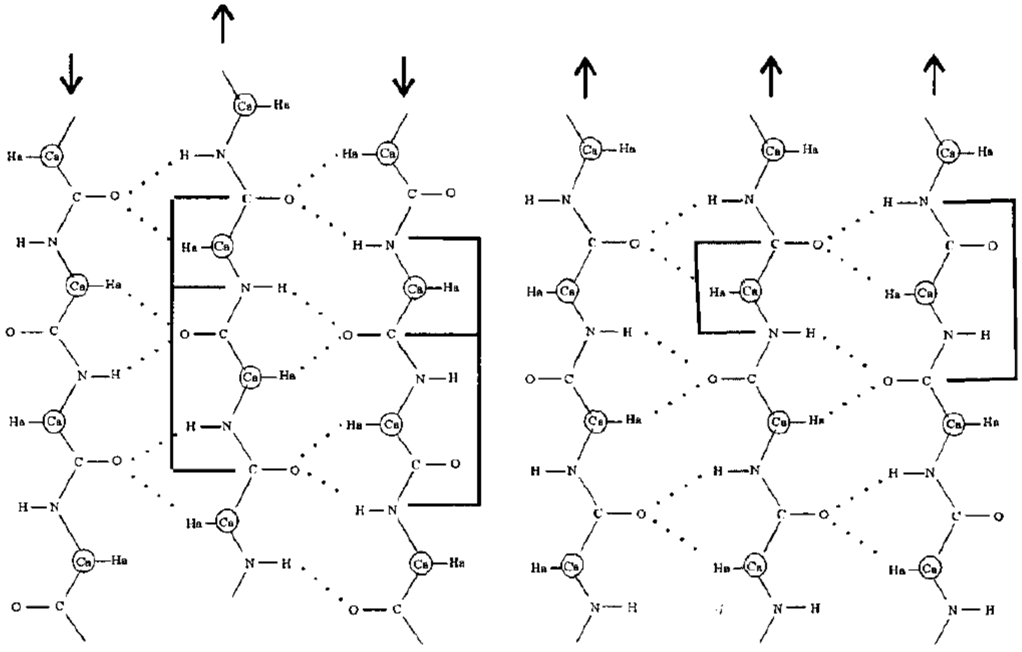

Figure 2.4: Anti-parallel and parallel beta-sheets, respectively[57].

Each of the three main secondary structure motifs has a characteristic signature in the Amide I band region of an IR absorption spectrum. The Amide I band region (1600-1700cm^{-1}) is the region of most interest due to the observation of protein secondary structures here. The random coil and alpha-helix are very similar, but are centred at different frequencies. Random coils are typically found between 1640 and 1650cm^{-1} and alpha helices are found in the region of 1640-1660cm^{-1}. This makes it difficult to distinguish between the two, however, the line shapes differ when compared[58]. The alpha-helix is centred around 1650cm^{-1} and has a shoulder around 1670cm^{-1}, whilst the random coil is centred around 1640cm^{-1} and is more rounded than the alpha-helix. Beta-sheets have two absorptions; one around 1630-1640cm^{-1}, which is typically the stronger of the two absorptions and a weaker band at around 1680cm^{-1}. The stronger absorption corresponds to the perpendicular vibration in the peptide chain, whilst the weaker band is the parallel vibration[30]. The orientation of these vibrations corresponds to the strands within the beta-sheet. The splitting of the band arises from Transition Dipole Coupling, which is a resonance interaction between two oscillating dipoles of neighbouring amide groups[59]. The Amide II, III and A bands surrounding the Amide I band are not useful for secondary structure analysis[1]. Amide II (~1550cm^{-1}) cannot easily correlate frequency with secondary structure. Amide III (1200-1400cm^{-1}) demonstrates influence from backbone and side-chain vibrations. Amide A (~3300cm^{-1}) is the NH stretching vibration and is not sensitive to the polypeptide backbone structure. Infrared Spectroscopy has been used for many years to observe the absorption of light in molecular vibrations and to determine secondary structure of peptides and model calculations performed to authenticate the findings[60]. 2DIR experiments are relatively new, in that they were first carried out around only ten years ago[61,62]. 2DIR takes an FTIR spectrum, and spreads it over an additional axis and provides structural and time resolution that is not available with FTIR alone. It has been the subject of recent review articles[7,63-65]. The use of 2DIR in the understanding of Amide I vibrations has also been reported[59,66].

FTIR spectroscopy is used to measure a spectrum of absorption of a molecule in steady state, or for slow reactions where the time scales of the reactions are much slower than the time for measurement. Atoms can be considered as two point masses held together by a spring (bond). The spring tension, or bond strength, affects the vibrational frequency. Therefore it can be described by an harmonic oscillator, but a more accurate approximation for the vibration of a diatomic molecule would be that described by the Morse Potential model, which was first reported in 1929[67] and considers the bond to be anharmonic and unlike the harmonic model, allows for bond dissociation. Figure 2.5 compares the harmonic and anharmonic oscillator, where r is the internucluear separation.

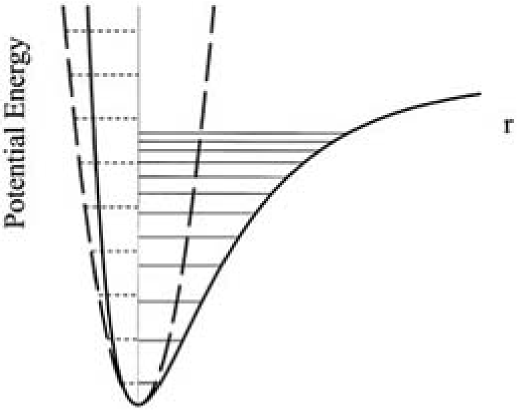

Figure 2.5: Comparison of harmonic and anharmonic oscillators[68].

It can be seen that the spacing of the vibrational energy levels in the anharmonic oscillator decreases as the potential energy increases. Molecular interactions are understood by measuring the effect interactions have on bond strength. This is gained using IR spectroscopy. Table 2.1 shows how vibrational frequency depends on both mass and bond strength. The greater the mass of attached atoms, the lower the IR frequency of absorption. The bond strength of the vibration increases the frequency.

Bond with dependence on atomic weight	Frequency (cm^{-1})	Bond with dependence on bond strength	Frequency (cm^{-1})
C - H	3000	C ≡ O	2143
C - D	2200	C = O	1715
C - O	1100	C - O	1100
C - Cl	700		

Table 2.1: IR Frequency is dependent on atomic weight and bond strength[23].

The optical density is a measure of how much light is absorbed by a sample, therefore, if it has a high OD, a lot of light is absorbed, and little transmitted. The absorption (A), or OD is related to concentration of the sample being probed via the Beer-Lambert Law;

$$A = -\log\left(\frac{I}{I_0}\right) = \varepsilon lc$$

Equation 2.1

Where I_0 and I are the incident and transmitted intensities, respectively. l corresponds to the length of path the light has to pass through the sample of concentration c. ε is the absorption coefficient, or molar absorptivity, of the sample. This coefficient describes how easily light can penetrate the medium in question. This coefficient is dependent on the wavelength at which the sample is probed at, the concentration of the sample and also has a dependence on the vibration-rotation transition of dipoles in molecules[69]. When two atoms in a molecule have considerably different electronegativities, the molecule has a permanent dipole. The intensity of absorptions depends on the size of the change in dipole. Barth and Zscherp[1] discuss the probability of a transition for a harmonic oscillator between two vibrational levels, *n* and *m* of the electronic state, ψ_0 by considering the Transition Dipole Moment, TDM. Equation 2.2 uses the Born-Oppenheimer approximation, separating the nuclear wavefunctions φ_n and φ_m from ψ_0. The dipole moment operator is $\boldsymbol{\mu}(t)$.

$$TDM = \langle \psi_0 \varphi_M | \mu | \psi_0 \varphi_n \rangle$$

Equation 2.2

For IR active vibrations, a change in dipole moment must occur during the vibration as described above. By splitting TDM into two terms; electronic and nuclear, two selection rules can be defined. The nuclear term is zero apart from $m=n\pm1$ and represents the selection rule that the vibrational transitions only occur to the next vibrational level, $\Delta n=\pm1$. The electronic contribution gives rise to the second rule, which says IR absorption can only occur when the dipole moment of the molecule changes with the vibration.

Time Resolved Infrared Spectroscopy

Variations in spectroscopic methods means different aspects of an interaction can be observed, i.e. steady state FTIR spectroscopy is used mainly where the sample does not change in time, or for “slow” reactions, i.e. $>10^{-3}$s. Whilst Step-scan FTIR can do experiments with reaction times on the nano-second scale. Time Resolved Infrared (TRIR) is used for fast, pico/nano-second, reactions by using a UV beam to excite molecules and an IR beam to measure changes in the spectrum, otherwise known as a pump-probe experiment. Here, FTIR and TRIR spectroscopy are used to examine reactions like the self-assembly of peptides, photo-triggered reactions and the protonation of a model protein active site. Other methods which could be used are UV-Vis absorption and fluorescence absorption to monitor molecular interactions, but IR spectroscopy is favoured since it gives structural information.

An FTIR spectrometer works in a similar fashion to a Michelson Interferometer, in that it consists of a beam splitter, a fixed mirror and a moving mirror. The light source is a globar, which is made from Silicon Bromide and is heated up to around 1898K[i], which emits Mid-IR light, which translates to the spectral region of 400-4000cm^{-1}. The beam splitter transmits half the radiation incident on it and reflects the other half. The radiation is therefore split into two beams; one is transmitted through the beam splitter to a fixed mirror whilst the other beam is reflected to a moving mirror. The mirrors reflect the radiation back to the beam splitter, where the beams are recombined, and the radiation passed through a sample. The light is then refocused onto a detector. The signal obtained is an interferogram which is converted to an absorption spectrum via Fourier transform operations performed by the computer. The FT splits the interferogram into its component waves. The signal detected is the time domain, and must be converted to the frequency domain via Fourier Transform;

$$S(t) = \int_{-\infty}^{\infty} I(v) e^{-iv2\pi t} dv$$

Equation 2.2

where *S(t)* is the signal in the time domain. The spectrum, *I(v)*, is obtained via

$$I(v) = \int_{-\infty}^{\infty} S(t) e^{iv2\pi t} dt$$

Equation 2.3

---

[i] http://www.kanthal.com

The optical path difference (OPD) is the difference in path travelled by the two beams through the interferometer. Absorption occurs when IR light interacts with the molecule, which will absorb energy, or photons and is excited to a higher vibrational energy level. The IR absorption spectrum has axes measuring Optical Density (OD, y) and Frequency (wavenumbers, cm^{-1}, x).

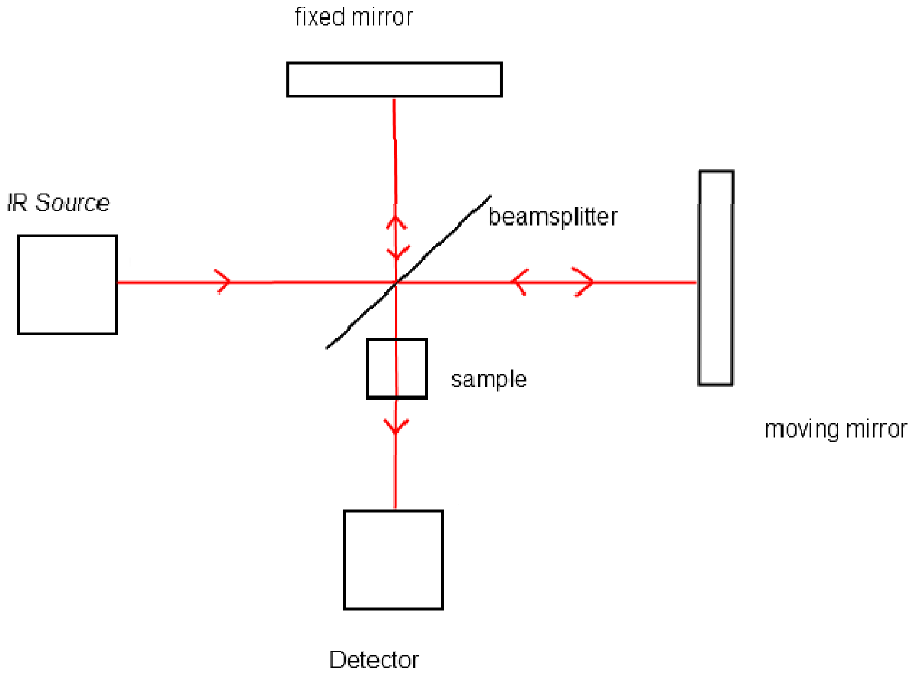

Figure 2.6: Schematic set-up of a Michelson Interferometer adapted for an FTIR Spectrometer.

If a sample of high concentration is to be probed, a short pathlength should be used, because the absorption, A, will be very high and so the light has a shorter path to travel through the sample. When the optical density exceeds approximately 2 absorbance units (AU) in the region of interest, the output spectrum becomes unreliable since the amount of light transmitted from the sample is a fraction of the incident light. Ideally, an AU of 1 should be maintained in all experiments to ensure accuracy. However, higher OD's have been recorded in some instances.

Whilst FTIR can provide structural information, it cannot provide time dependent measurements due to limitations on the scan/detector time. There are other techniques which allow a time-dependence to be established. Step-scan FTIR is useful for following reaction on short time scales, a short as 12ns, which is a limitation due to the instrumentation, but is still much faster than standard FTIR. Data recorded in an FTIR experiment are collected at discrete positions of the movable mirror. For a step-scan experiment, movement of the mirror is stopped, where the Optical Path Difference (OPD) stays constant for a short time. A time-resolved experiment is performed at this position. The mirror then moves to the next position and the experiment is repeated. This technique is most useful for following photo-chemical reactions triggered by a laser pulse. The time between the collection of each spectrum is around 10ns. This makes it ideal for following reactions on short time scales, allowing changes to be observed easily. However, for faster reactions this method cannot be used due to limitations on the apparatus, therefore a technique like TRIR spectroscopy would be used.

TRIR spectroscopy employs a pump-probe technique which consists of a UV pump beam, which is used to excite the molecules, and an IR probe. Pump-probe experiments do not always consist of a UV pump-IR probe. A different combination may be used depending on the wavelength that excites a molecule. There are reports on the theory behind IR pump-probe spectroscopy[70,71] which discuss the use of the technique for photo-chemical reactions. The probe pulse measures the IR absorption of the sample by probing vibrational transitions, whilst the UV pump pulse excites electronic transitions. By exciting these electronic transitions, changes in the IR spectrum are recorded. Differences in the spectrum caused by electronic excitation are measured by recording the IR probe spectrum with and without the presence of the UV pump pulse. The difference is calculated by subtracting the initial probe spectrum from the subsequent spectrum, so the changes undergone after the UV excitation can be observed. During the time delay between the IR and UV beams, some electrons relax to the ground state.

Fast, micro- and nano-second mechanisms like protein folding, can be studied with this system. Structural information and kinetics can be extracted from a TRIR spectrum. For nano-second TRIR experiments, the set up shown in Figure 2.7 was used. An OPA (optical parametric amplifier) consists of a nonlinear crystal which is used to emit light of variable wavelength; in this case it is mid-infrared, which has 3-8µm wavelength and a kHz repetition rate. This was seeded by a 65Mhz Ti:Sapphire oscillator. A UV pump pulse was produced by a frequency tripled Nd:YAG laser matching the repetition rate of the IR probe pulse. The chopper works at half this frequency to modulate the UV pump beam. A computer-controlled delay generator was used to determine the time delay between the pump and probe beams. The mirrors on the IR beam line are made from gold coated glass. The fact they are gold coated means they have optimised reflectivity in the mid-IR range. Lenses are typically made from CaF_2. The mirrors on the UV beam path are dielectric, which means they can be designed to have a specific reflectivity at certain wavelength in particular. This allows the beam to be tuned to the ideal wavelength to excite a sample.

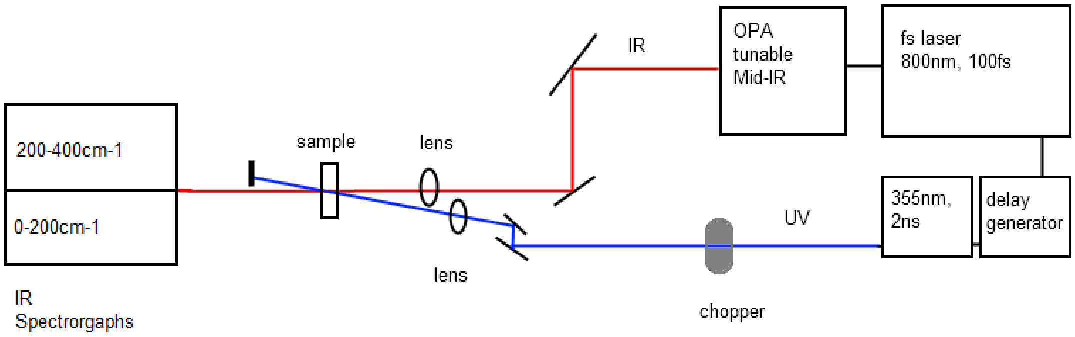

Figure 2.7: Schematic of the nano-second set up for TRIR spectroscopy.

For working in the pico-second time scale, a different TRIR set-up was used, as shown in Figure 2.8, which is used for very fast reactions. This is because the pulse duration and the time delay between the pump and probe beams must be shorter in order to observe the faster reaction. The OPAs are pumped by the 800nm laser to produce the pump and probe beams. The UV beam passes through an optical delay line which aids in creating a short time delay between the pump and probe. This time delay is created by increasing the path the IR pulse has to travel. As before, the optical chopper modulates the UV pulse to half the repetition rate of the laser. The signal is detected on the IR spectrographs, which consist of a spectrometer-array detector combination[49].

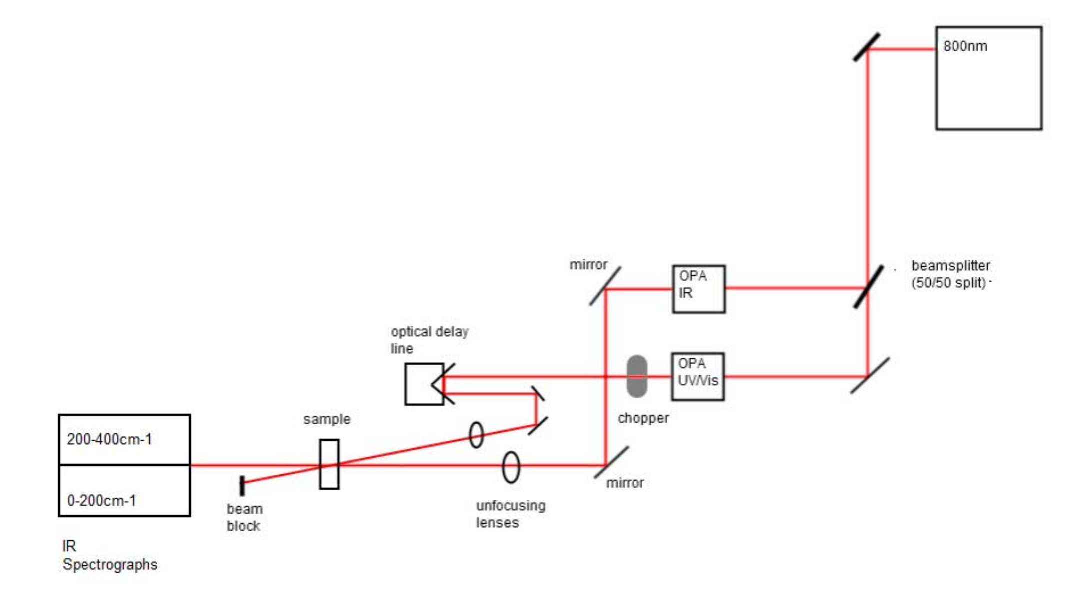

Figure 2.8: Schematic of the pico-second TRIR set-up.

Typically, a narrow-band pump pulse and broad-band probe pulse are used. A narrow pump pulse allows certain vibrational modes to be excited. Probing with a broad-band pulse provides a wide area in the spectrum to be examined. The data gathered from a TRIR experiment is recorded across two detectors, which were tuned to detect the signal from merging frequency ranges, therefore overlapping the data. Each detector records a 200cm^{-1} range. To merge the data from the two spectrographs into one, common features between the two were lined up and known features from the steady-state FTIR spectrum were identified. The spectrographs record data in pixels, which must be converted to wavenumbers. This is carried out by identifying points on the TRIR spectrum which matched on an FTIR spectrum. A small number of points were chosen along the spectrum and plotted, pixel number against wavenumber and fitted with a line of the form *y=a+bx*. The wavenumber is then found by substituting the pixel number as *x* and the intercept and slope of the fitted line. The resulting spectra are in the form of a difference spectrum.

All samples, unless otherwise stated, were prepared in an air tight glove box in order to eliminate the absorption of water from the air. H_2O absorbs strongly in the Amide I region, at 1650cm^{-1} as well as in the region above 3200cm^{-1}. In an FTIR spectrum this means the absorption from this is produces a high OD, rendering the spectrum ineffective, as the absorptions observed in the Amide I band can no longer be distinguished. The FTIR Spectrometer was purged with “dry air” to eliminate water absorption during the experiments. Once prepared, samples were loaded between two calcium fluoride (CaF_2) windows separated by a Teflon spacer. These were held in place using a Harrick Cell which slots into the sample holder in the beam path. The correct pathlength could be calculated using Equation 2.1 to ensure the ideal O.D. is achieved. For photo-chemical reactions undertaken in with the FTIR spectrometer, a UV lamp was used as the source. The sample was held close to the lamp for a set amount of time to ensure total exposure. FTIR spectra were obtained using a Bruker Vertex 70 Spectrometer. The spectral resolution of FTIR spectra was 1.5cm^{-1}. UV-Vis spectra were obtained using a Shimadzu UV-2501PC Spectrophotometer, and had a spectral resolution of 1nm.

Chapter 3: Self-Assembled Peptides

Introduction

The self-assembly of peptides is a much studied area due to the structural similarities with neuro-degenerative diseases like Alzheimer's, Parkinson's and Huntington's disease which result from the mis-folding or aggregation of polypeptides[2,72], leading to the formation of amyloid fibrils. It has been suggested that synthetic peptides may form amyloid fibrils under the correct conditions, meaning there are potentially a general set of rules for amyloid fibril formation[73]. To understand the mechanisms of the fibril formation process which lead to these degenerative diseases, they can be modelled under laboratory conditions using self-assembly peptides. Another application of self-assembling peptides is the construction of nanomaterials for tissue engineering[35,74,75], because they can act as scaffolds for cell cultures and can promote cell proliferation. As well as this, they can also be used in the fabrication of biosensors[76]. A biosensor uses living organisms or biomolecules to detect the presence of bacteria or toxins in the environment and in humans. Non-biological applications include nano-electronics, where the self-assembled nano-tubes can be used as a template for making nano-wires[40] and also for use as biodegradable drug carriers[77]. These self-assembled systems are of interest due to their chemistry-rich structures as well as their compatibility to biological systems.

Self-assembly systems are often analysed using transmission electron microscopy[38,39] (TEM) which uses a beam of electrons transmitted through a thin sample. An image of the interaction of the transmitted electrons with the sample is produced. The image is used to determine the type of structures that have been formed, i.e., nanotubes or ribbons; however this does not give information on how the nano structures are formed, which IR spectroscopy can give. Circular dichroism (CD) is another method which can be used for examining self-assembling structures. It can provide information on the fraction of the molecule that is in a certain conformation. Infrared (IR) spectroscopy offers information on molecular vibrations by enabling the identification of the conformation as described in detail in *Chapter 2*. It is important to observe self-assembled systems over a time period since they may not take a direct path to their final assembled form, and so the reaction must be observed for the duration. These reactions can take many hours to complete. Self-assembled systems constructed from water take the form of a gel. The gel is formed because the molecules have aggregated.

The *Oxford Dictionary of Biochemistry and Molecular Biology* defines self-assembly as: "the formation of a complex entity from more simple, identical units without intervention from any external agency". It is possible to control self-assembly via a pH trigger. Peptides can be designed to have a fibril state at low pH and monomeric state at high pH[78]. This offers a way for direct and controlled production of a gel from monomeric peptides. Self-assembly is driven by a thermodynamic process which aids the procedure. The system is in dynamic equilibrium, which means there is an equilibrium between the monomeric components and the aggregated complex[79]. In other words, the ratio of reactants and products remains the same and although reactions are occurring, they may not be observable with time-resolved spectroscopy. The equation of equilibrium for the formation of a self-assembled structure states;

$$\Delta G_{self-assembly} - \Delta G_{amide-hydrolysis} \prec 0 \qquad \text{Equation 3.1}^{80}$$

where G is the free energy of the system. This equation can be explained with the aid of Figure 3.1, which shows how the energy of the system changes as the self-assembly process develops over time.

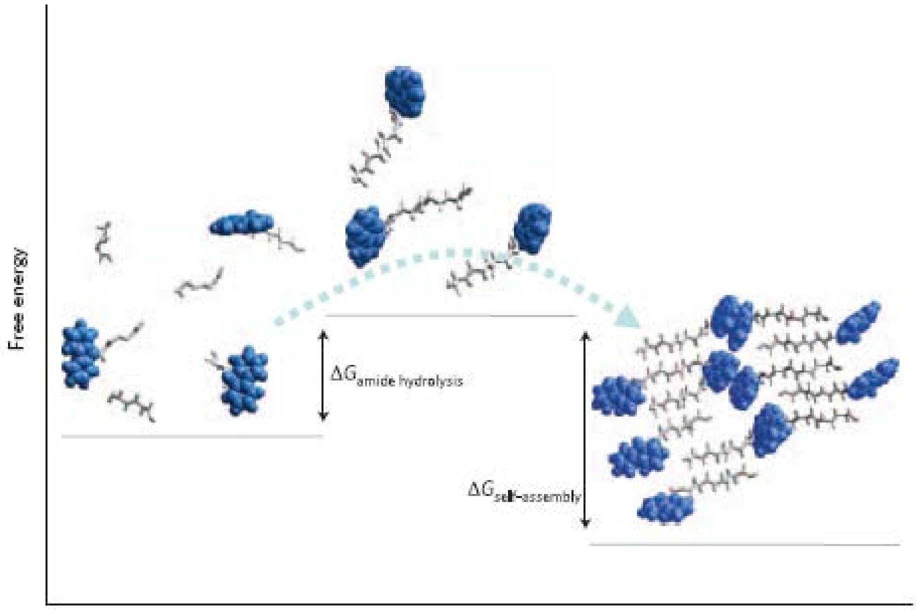

Figure 3.1[ii]: Free energy diagram of an enzyme assisted self-assembly. Fmoc group is shown in blue, whilst the peptide units are grey.

The Gibbs Free Energy of the system is related to entropy via Equation 3.2;

$$\Delta G = \Delta H - T\Delta S \qquad \text{Equation 3.2}$$

where ΔH is the change in enthalpy of the system and T and ΔS are the thermodynamic temperature and change in entropy, respectively. In an enthalpy-driven process, ΔS is expected to be negative. The only way to ensure ΔG is negative, is the change in enthalpy, ΔH, must be negative and of sufficient magnitude so that the addition of a positive $(-T\Delta S)$ value produces a negative ΔG. The negativity of ΔH is a result of the formation of weak bonds, and represents a loss of potential energy in the system. For the system to be entropy-driven, ΔH would be positive and to make sure ΔG is negative, ΔS must be large and positive such that $(-T\Delta S)$ added to ΔH generates $-\Delta G$. This positive value of ΔH does not pertain to the formation of bonds, but either to the breakage of bonds or bringing equal electrical charges close to each other. ΔS is a measure of disorder in the

---

[ii] Taken From: (80) Williams, R. J.; Smith, A. M.; Collins, R.; Hodson, N.; Das, A. K.; Ulijn, R. V. *Nature Nanotechnology* **2009**, *4*, 19.

system during self-assembly[79-81]. Therefore, self-assembly must be an enthalpy-driven process since the change in entropy associated with ordering will be negative.

The self-assembly of molecules occurs when there is a covalent link between amino acids of one molecule to another by forming peptide amphiphiles or π-π interactions between aromatic rings[40]. Amphiphilic compounds are both hydrophobic and hydrophilic at the same time. In amphiphilic beta-sheets, peptide residues are usually alternated hydrophobic and hydrophilic. The self-assembly of amphiphilic peptides is assisted by interactions between hydrophobic residues in aqueous environments[56]. π-stacking is a noncovalent interaction between two compounds that possess aromatic rings and is formed through the overlap of orbitals. π-orbitals occur when two p-orbitals overlap on adjacent atoms. Fluorenylmethoxycarbonyl (Fmoc) based dipeptides are motivated by the attractive interactions between π electrons on the fluorenyl rings[36]. Anti-parallel β-sheets are also formed in the peptide formation. π-stacking takes place in the self-assembly system, and the time scale by which these two processes occur must be determined. Figure 3.2 shows a schematic diagram of the stacked structures and the formation of beta-sheets.

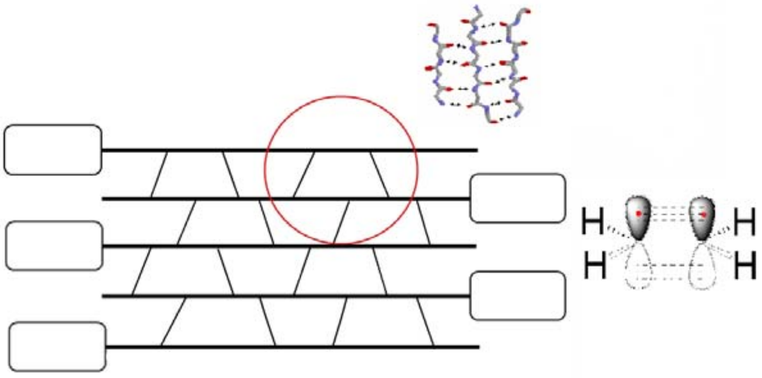

Figure 3.2: Schematic of π-stacking between Fluorenyl groups[iii,iv]

[iii] Beta sheet: http://cryst.bbk.ac.uk

[iv] Pi bond: http://chemwiki.ucdavis.edu

The system forms a hydrogel via aggregation as the molecules come together, forming Hydrogen bonds. In the experiment considered here, where a hydrogel is formed, the aim is to produce a thorough analysis of the self-assembly process, which has been previously observed via HPLC (High Performance Liquid Chromatography), Fluorescence Spectroscopy and TEM (Transmission Electron Microscopy)[38,39,82]. It is hoped that using IR and UV-Vis Spectroscopy to observe the process will give insight into the secondary structure of the molecules throughout the reaction and an understanding of the π-stacking interaction previously identified. The mechanisms are not observed using only one Spectroscopic technique, hence the need to use both FTIR and UV-Vis Absorption Spectroscopy. FTIR Spectroscopy probes the vibrational properties of amino acids, which are sensitive to changes in molecular structure[83]. Multiple spectra are obtained and a comparison via difference spectra shows the structural change of the molecular structure over time. UV-Vis Absorption spectroscopy measures the amount of light absorbed by the sample in that region. In Fluorescence Spectroscopy experiments of a similar system to that examined here, stacking interactions were observed as a shift to longer wavelength[39]. The wavelength of the absorption is dependent on the amount of delocalisation in the molecule. This is when unpaired electron density in the molecule is spread across several atoms. To understand this system, the process involved with the self assembly must be investigated to determine how it achieves its final state, which is the most stable both structurally and thermodynamically.

Experimental Details

The system considered here consists of Fmoc-Threonine (Fmoc-T), Phe-oME (Phenylalnine with a methyl ester group) and the enzyme, Thermolysin. This enzyme is used to aid the formation of peptide bonds through reverse hydrolysis. The molecular structures are shown in Figure 3.3.

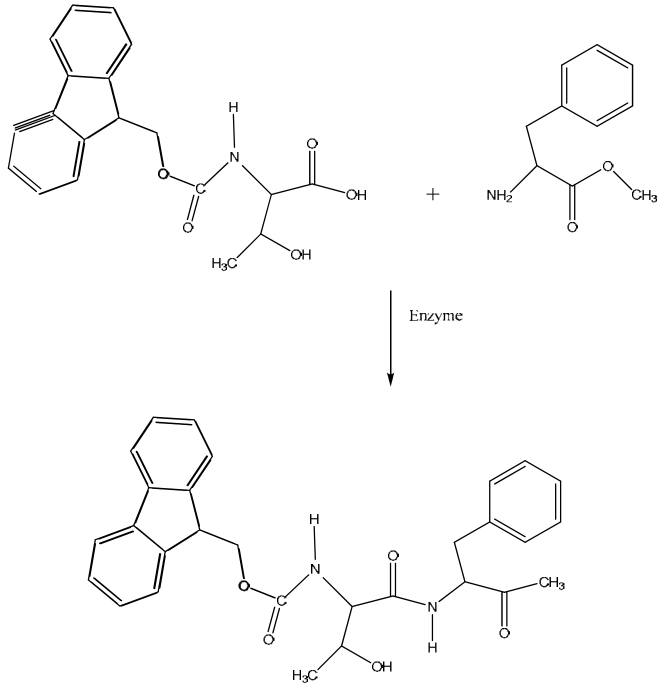

Figure 3.3: Fmoc-T + Phe-oME + Enzyme and the product.

Samples were prepared in a phosphate buffer. 7.83mM NaH_2PO_4 was added along with 117.21mM Na_2HPO_4 to 10ml D_2O. The monomers, Fmoc-T and Phe-oME, were mixed together with a concentration of 21mM and 90mM, respectively in 1ml D_2O. The enzyme of concentration 0.014μM was added to 1ml of the buffer. These two solutions were then added together to produce the final suspension.

In the early stages of the experiment, it was found that mixing Fmoc-T, Phe-oME and the enzyme together at once created solubility issues with both Fmoc-T and Phe-oME, and results obtained were not reliable or reproducible. This meant a new method of preparing the sample was required. Through trial and error, it was found that mixing the monomers separately to the enzyme ensured they all dissolved properly in solution. These two solutions were then added together, and agitated for 30 seconds. This method of mixing gave more accurate and reproducible results, which are described here. Figure 3.4 shows the states in which the initial suspension is a clear liquid and as time passes, the consistency of the sample becomes that of a gel and is visibly opaque. The vial is turned upside down to show that the sample is in the form of gel (indicated by the arrow) and does not flow freely within the vial.

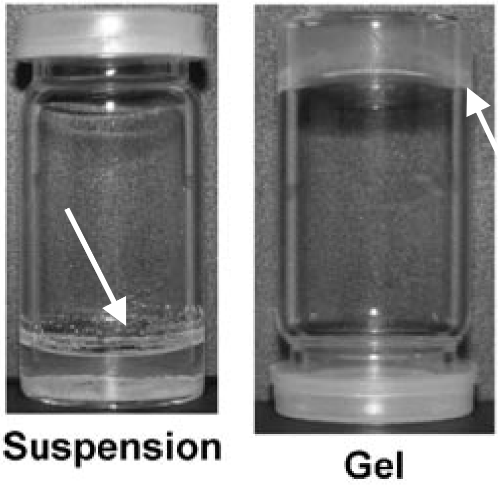

Figure 3.4[v]: Photo of the initial suspension and the gel that is formed.

The reaction was followed using FTIR and UV-Vis Spectroscopy. The time intervals between data collection were set at every five minutes in the first forty minutes, and every twenty minutes for twenty-four hours, thereafter. The time for the experiment was set to this because previous HPLC (High Performance Liquid Chromatography) measurements found that similar reactions to that depicted in Figure 3.3 took approximately this amount of time to complete[82]. HPLC experiments are used in separating chemical compounds. In the FTIR experiment, 124 interferograms were collected in each measurement with a spectral resolution of 1.5cm^{-1}. This allowed measurements to be taken in quick succession yet maintain good spectral resolution for analysis. Samples were loaded between two CaF_2 windows with a pathlength of 25µm for both FTIR and UV-Vis measurements. For consistency between the two methods, the gel solutions were taken from the same prepared sample. Although not considered here, the reaction could also be followed via Fluorescence spectroscopy, which is complementary to UV-Vis Absorption spectroscopy. Fluorescence spectroscopy measures the emission of light from a sample which has absorbed light of a different wavelength, whereas

---

[v] Taken from: (39) Das, A. K.; Collins, R.; Ulijn, R. V. *Small* **2008**, *4*, 279.

UV-Vis Absorption spectroscopy measures the amount of light absorbed by a sample. For this reason, it is not considered here.

Experimental blanks, where the suspension was prepared without the addition of the enzyme. Figure 3.11 shows the FTIR and UV-Vis spectra of this. Further spectra were obtained and it was clear that the enzyme was required for the self-assembly process to occur.

Results and discussion

FTIR spectra of the monomers were obtained so that absorption peaks in further analysis of the full reaction could be identified. Figure 3.5 shows FTIR spectra for the two monomers in a 1:1 D_2O:Acetonitrile solvent. This solvent was used since it does not show a spectroscopic contribution in the Amide I band.

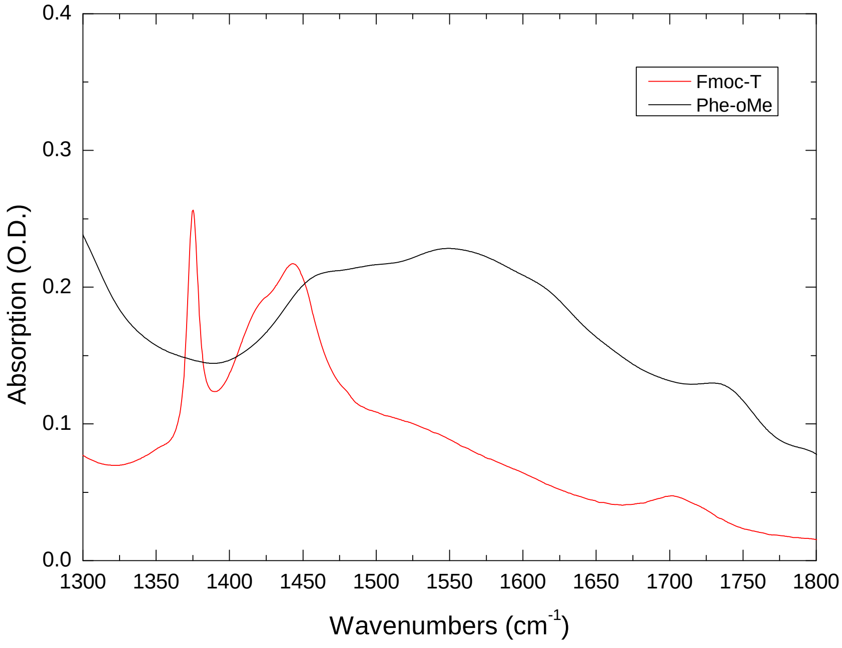

Figure 3.5: FTIR spectra of Fmoc-T and Phe-oMe.

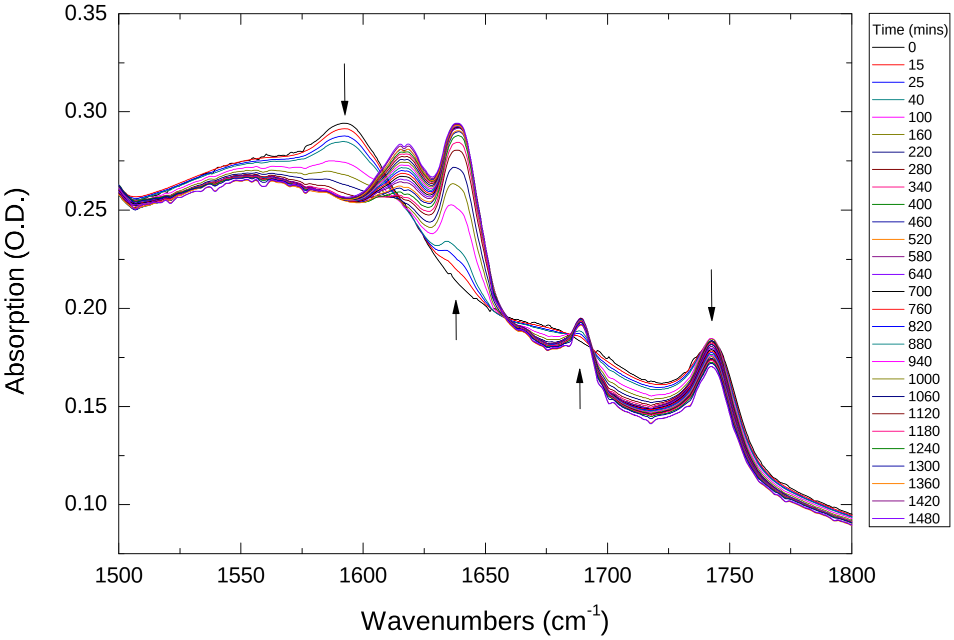

Figure 3.6: FTIR spectra of the full reaction gathered over 24 hours.

As can be seen from Figure 3.6, some features appear in the Amide I region (1600-1700cm^{-1}), and others disappear during gel formation as indicated by the arrows. This can be shown more clearly by creating a difference spectrum, where the initial measurement is subtracted from the subsequent data sets to present a change in the spectrum with each measurement. This is shown in Figure 3.7. The features at 1639 and 1689cm^{-1} are consistent with the appearance of beta-sheet structures[30]. 1595cm^{-1} may be a peak associated the loss of the NH_2 scissor stretch[84]. The peak at 1742cm^{-1} appears to be due to the CH_3CHO(84) which comes from the Fmoc-T monomer, as seen in Figure 3.3. Further measurements were carried out on the monomers alone, allowing the spectral features to be assigned to them. The peak at 1620cm^{-1} is due to the formation of an intermolecular beta-sheet.

Spectrum Position (cm^{-1})	Assignment	Reference
1595	NH_2 scissor stretch	84
1639, 1689	Signature of β-sheet	1,30,85,86
1742	CH_3CHO from Fmoc-T	84

Table 3.1: Spectral positions, assignment and literature reference.

Table 3.1, above, lists the peaks of interest, their vibrational assignment and the literature references which provide evidence of these assignments. These features were chosen for further analysis because primarily, they are in the Amide I band region which provides crucial structural information. NH stretches can be observed in the Amide A band (~3300cm^{-1}) but this region is not sensitive to backbone structure.

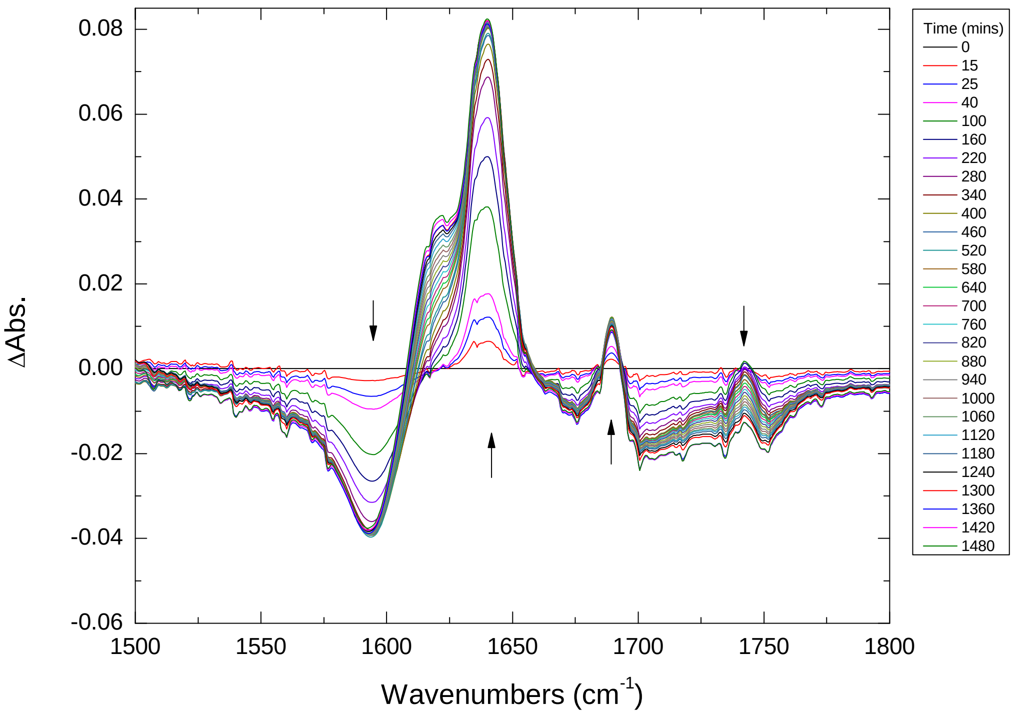

Figure 3.7: Difference FTIR spectra for the total reaction.

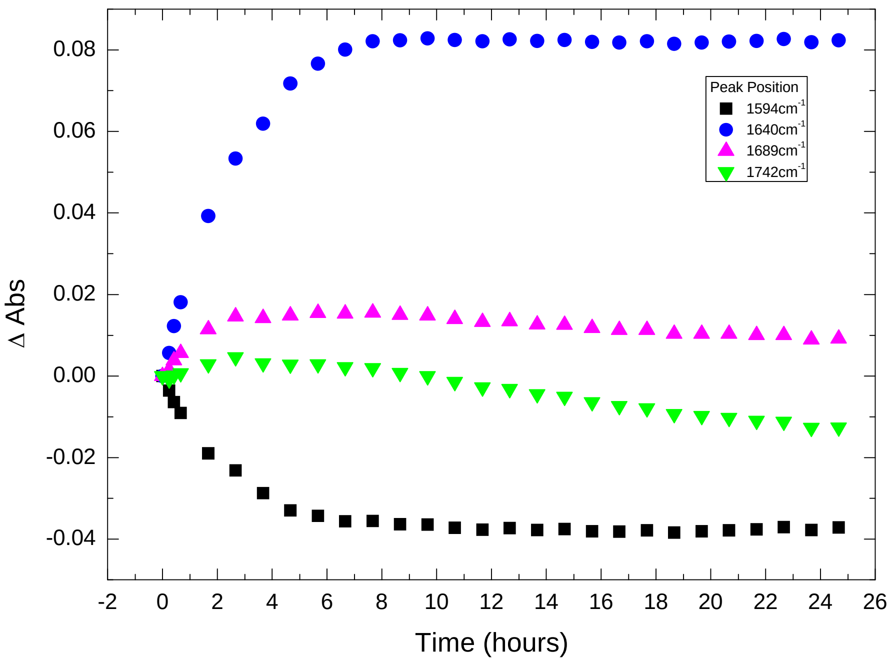

Figure 3.8: Kinetics of peaks indicated.

The complex nature of the baseline associated with the spectra in Figure 3.7 meant that a correction had to be performed. A point was chosen at either edge of the region of interest in each spectrum. The software used for data analysis produced a baseline function for each spectrum between these two points. An average of the y-value for the two chosen points was obtained as a correction factor, and was then subtracted from each spectrum.

Taking a plot of kinetics at the peaks indicated, Figure 3.8 can be produced. By fitting exponential functions to the kinetics of the peaks 1594, 1641 and 1689cm^{-1}, the time of the formation or loss of features can be examined. Figures 3.9 and 3.10 shows these fits.

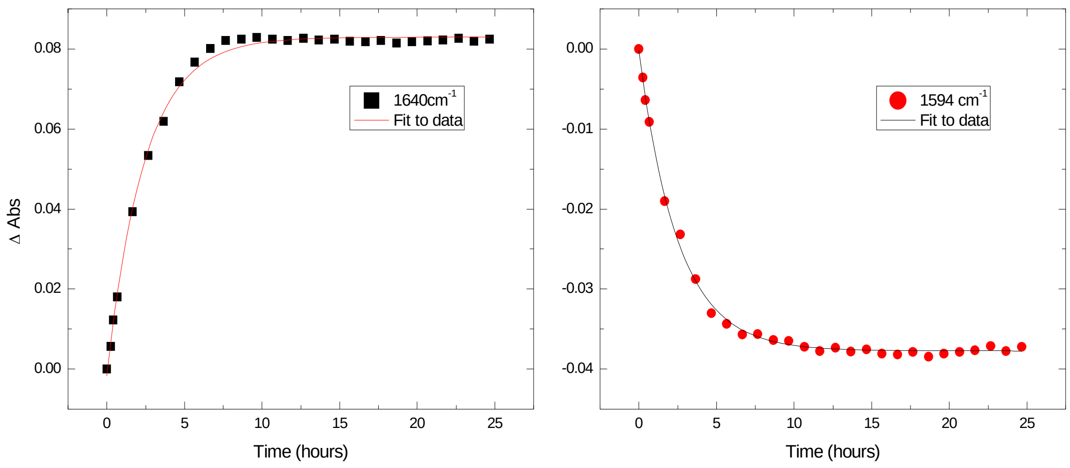

Figure 3.9: Fits to peaks 1594cm^{-1} and 1641cm^{-1}.

The graph shows that the peak of 1641cm^{-1} which corresponds to the strong absorption band of the anti-parallel beta-sheet, has a growth constant of 2.424 ± 0.066 (hours) and the 1594cm^{-1} peak, has a decay constant of 0.399 ± 0.010 (hours). The weak absorption band of the anti-parallel beta-sheet at 1689cm^{-1} has an initial time constant of 0.516 ± 0.020 (hours), shown in Figure 3.10. Table 3.2 displays the time constants for the three fitted curves, as well as R^2 data for each. The value of R^2, the coefficient of determination, provides an evaluation of the goodness of fit of the data. The closer this value is to 1, the better the fit to the data.

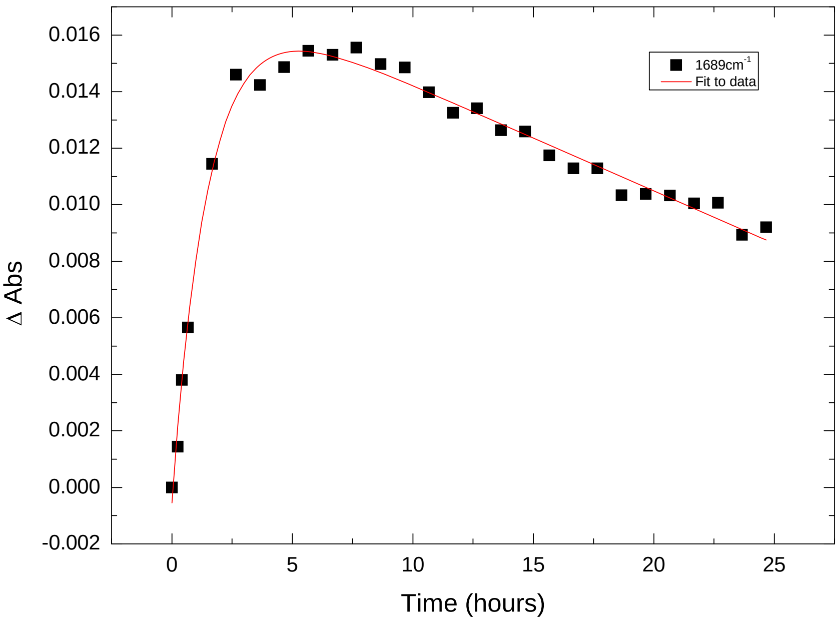

Figure 3.10: Fit of the 1689cm^{-1} peak.

Wavenumber (cm^{-1})	1594	1641	1689
Time constant	0.399 ± 0.010	2.424 ± 0.066	0.516 ± 0.020
R^2	0.997	0.997	0.988

Table 3.2: Time constants for fitted data.

UV-Vis Spectroscopy was also undertaken to observe the development of π-stacks. Measurements were gathered between 250-500nm, which is the ultraviolet region, leading into the visible region. The position of peaks observed in UV-Vis Spectroscopy shows the wavelength at which the molecule is excited. When the molecule absorbs light, transitions between the electronic states are induced. Therefore, if a molecule absorbs at a certain wavelength, there is a certain amount of energy associated with the absorption. As the electrons become more delocalised, the wavelength of absorption increases, which is what is observed as π-stacking occurring. The change in wavelength is due to a shift in energy levels caused by the mixing of π-orbitals upon stacking, leading to an increase in the wavelength of the absorption.

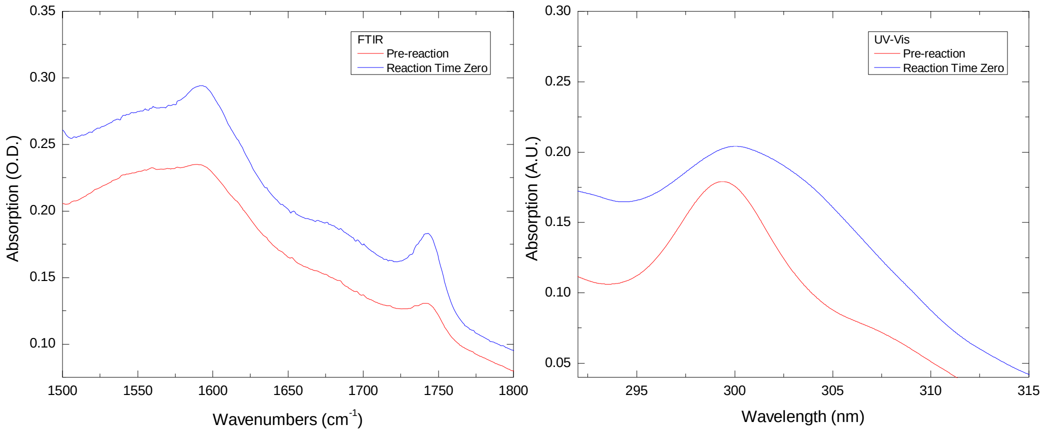

Figure 3.11: Comparison of before and after the start of the reaction via FTIR and UV-Vis.

Figure 3.11, above, shows FTIR and UV-Vis spectra of the full reaction at time zero, and also ‘pre-reaction’, i.e. the reaction mixture minus the enzyme.

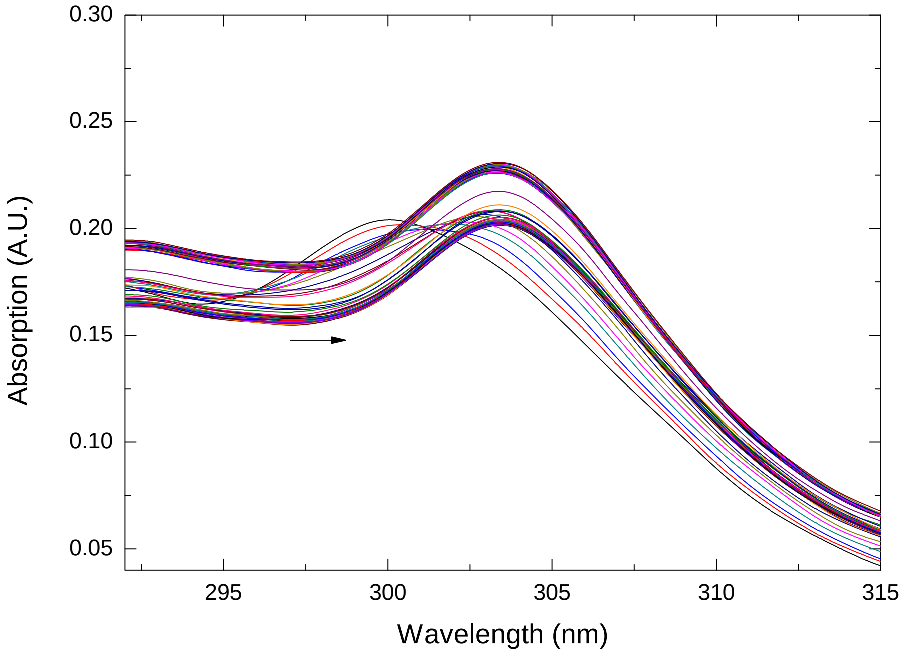

Figure 3.12: UV-Vis spectra of the full reaction.

Figure 3.12 shows the change in the UV Spectrum as time passes. The change in peak position from 300nm to 303nm happens very quickly, compared to changes observed via FTIR. Fitting this data with an exponential, Figure 3.13, gives a rise time of 10.59 ± 1.89minutes, which is considerably faster than that noted in the mechanisms observed via FTIR. Evidence of π-stacking interactions in the fluorenyl groups of the proposed structure has been observed via Fluorescence Spectroscopy and is recorded as a shift to a longer wavelength in the spectrum[82]. This shift is also observed in the UV-Vis data presented, which leads to the conclusion that this is evidential proof of π-stacking. The point in the graph for the peak position of 304nm is ignored since it is clear the data plateaued at the same value before and after this point.

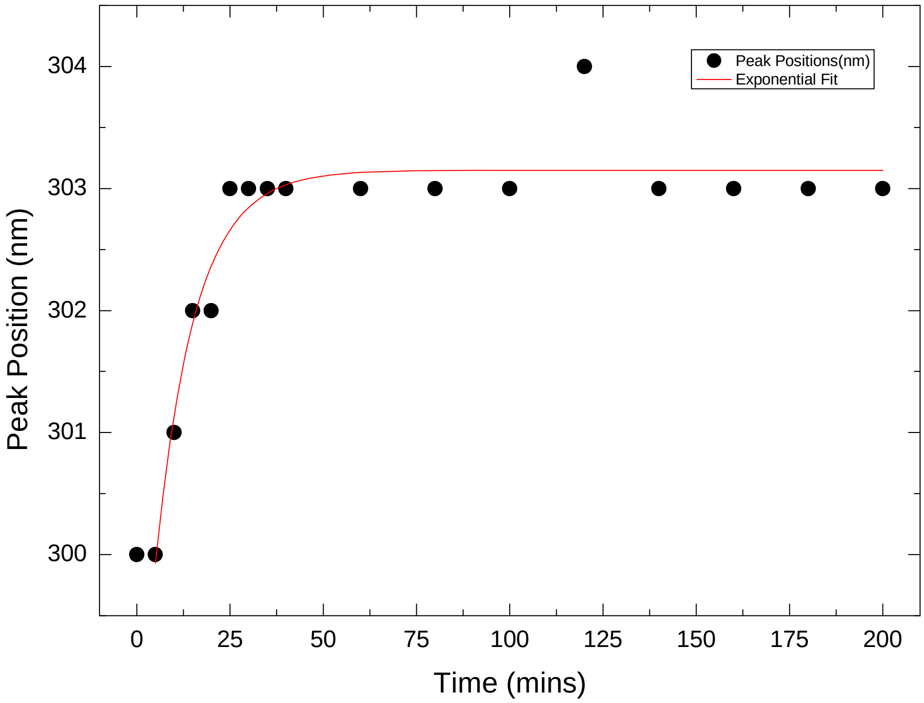

Figure 3.13: Plot of change in peak position, fitted with an exponential.

The time scale for π-stacking interactions is much shorter than that of the formation of beta-sheet structures. The π-stacking occurs within ten minutes of the beginning of data collection and the formation of beta-sheet structure is within approximately two hours. The process of π-stacking and the formation of beta-sheets are thermodynamically favourable and give the most stable state assumed by the molecule.

The relative strength of the peptide bonds and interactions of the π-stacking are weak, but having many of these bonds and interactions helps stabilise the structure[33]. This suggests the system is enthalpy-driven; meaning the change in entropy of the system is negative. An enthalpy-driven system suggests that the formation of peptide bonds is the driving force for the stacking process. If the change in entropy had been positive, as stated earlier, it would not relate to the formation of bonds in the system.

Previous work on this system has shown that a hydrogel is formed within an hour of the addition of the enzyme, Thermolysin[39]. As shown in Table 3.2, the loss of the NH_2 scissor stretch has a decay time of 0.399 ± 0.010 hours. In this time, the peptide has formed and molecules of water have been produced, i.e. the gel is formed. Evidence for the formation of π-stacks in the system was observed to occur with a rise time of around ten minutes, as shown in Figure 3.13. It has been reported to occur within the first 96 hours of addition of the enzyme to the experiment, as observed via Fluorescence Spectroscopy, where an initial spectrum was obtained and another after 96 hours[82]. This was determined due to the time taken for an equilibrium state to be reached for conversion to a gel-state.

The growth and decay of peaks do not occur within the error band of each other. This suggests several processes are occurring at once. The more intense band of the beta-sheet takes much longer than the less intense peak to develop fully. The data suggests π-stacking of the system is the first to occur, as seen by UV-Vis, in 10.59 ± 1.89 minutes. This is followed by the loss of the NH_2 stretch after 0.399 ± 0.010 hours (approximately 24 minutes). The formation of beta-sheet content then begins after approximately 30 minutes and lasts for a further 2 hours.

Conclusions

The understanding of the self-assembly of peptides is important because the way in which the assembly process proceeds, and the formation of fibrils is comparable to the formation of amyloid fibrils which leads to the development of neuro-degenerative diseases. With an understanding of the formation under laboratory conditions, preventative measures can be taken to avoid the formation of these fibrils, which could be controlled thermodynamically, as in Figure 3.1.

Future work on this system would be to use 2D-IR Spectroscopy to observe the self-assembly process. It would be useful for this, as the vibrational coupling of modes is observable in 2D-IR spectra. Some systems have already been observed using 2DIR Spectroscopy[72], with a view to understanding the kinetics in more detail in order to be able to simulate the aggregation process.

The system analysed here is enzyme-triggered, but other self-assembly systems can be triggered by exposure to light[87] or a change in pH[78,88,89] which would see the change of protein structure, and ultimately function.

Chapter 4: Photochemistry Of o-Nitrobenzaldehyde And Applications To Model Enzyme Systems.

4.1 o-Nitrobenzaldehyde

Introduction

This chapter will focus on the use of a photoacid as a trigger in pH-induced reaction, where the molecules involved respond to a change in the pH of the environment.

In this study, the photoacid will be used to alter the conformation of a model polypeptide system in a helix-to-coil transition where altering the pH of the environment changes the charge of the side chain and hence causes the secondary structure to modify to the more thermodynamically favoured conformation. It will also be used to aid the protonation of a model Hydrogenase enzyme system. These model Hydrogenase systems are used to catalyse the production of molecular hydrogen. These applications are of interest because the use of time-resolved IR spectroscopy allows reactions to be followed; to observe changes in secondary structure due to pH changes[90], and also to determine how protonation of the hydrogenase system leads to the development of molecular hydrogen.

Firstly the dynamics of the photoacid itself must be understood. FTIR (Fourier transform infrared) and TRIR (time resolved infrared) spectroscopy studies were carried out on the photoacid to provide information on the intermediates of the photoacid during a reaction. The photoacid's role as a proton donor is only activated once it is exposed to ultraviolet (UV) light. When exposed to UV light, the photoacid releases protons which in turn increases the concentration of $[H^+]$, decreasing pH. The photoacid considered here is o-nitrobenzaldehyde, oNBA, which is known to undergo a reaction in converting from a nitro acid to nitroso acid in both solid state and solution[47,91,92]. This has been studied previously[47,93] using flash photolysis, where a sample is exposed to a short, powerful flash of light triggering the start of the chemical reaction. The resulting spectra are used to identify photo products via absorption or fluorescence, but techniques have improved over time and a more in depth investigation, benefiting from improved time resolution, is possible[45,46].

oNBA consists of an aldehyde (O=C-H), which converts to carboxylic acid, a weak acid and nitro group (NO_2) which converts to a nitric oxide group after UV exposure. Other photoacids may not be as efficient in a photo-reaction as oNBA is i.e., the conversion of oNBA to nitrosobenzoic acid provides a high quantum yield[44].

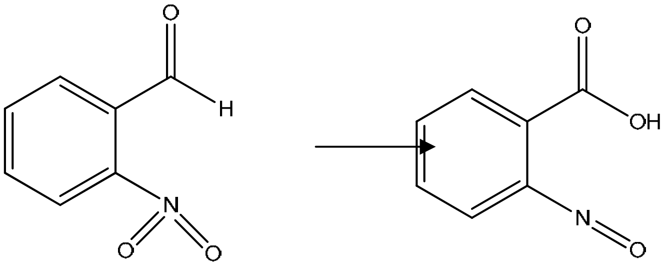

Figure 4.1: oNBA in its initial form, and nitrosobenzoic acid, the form it takes after UV illumination.

It is believed that as the photoacid undergoes the transformation to its final state, as nitrosobenzoic acid, it assumes an intermediate in the form of a ketene[46]. The photoacid is being studied here to determine the dynamics of the photoreaction under conditions not previously considered. oNBA has been studied previously using acetonitrile and ethanol as the solvent, and data was collected using Raman, absorption and femtosecond IR spectroscopy. The lifetime of the ketene intermediate has been shown to have a strong dependence on solvent[44,45,93]. It has been reported that the ketene intermediate is formed within 0.4ps of UV excitation, and has a lifetime of 90ps in ethanol[44]. In a 1:1 ethanol:water mixture, this lifetime was found to be 13ps. The presence of water clearly accelerates the transition from ketene to carboxylic acid. Water is slightly more acidic than ethanol, and so this suggests that water donates a proton to the OH group which converts to acid. Since ethanol is a protic solvent, it is possible that it forms an intermolecular hydrogen-bonded complex with the o-NBA parent molecule[94]. In a Raman experiment, with acetonitrile used as the solvent, the ketene intermediate was reported to have a lifetime of 10ns which is consistent for data presented for IR spectroscopy[45]. Here, the solvents used are acetonitrile and a mixture of D_2O and deuterated methanol. D_2O and methanol-D_4 were used as they could increase the solubility of the photoacid.

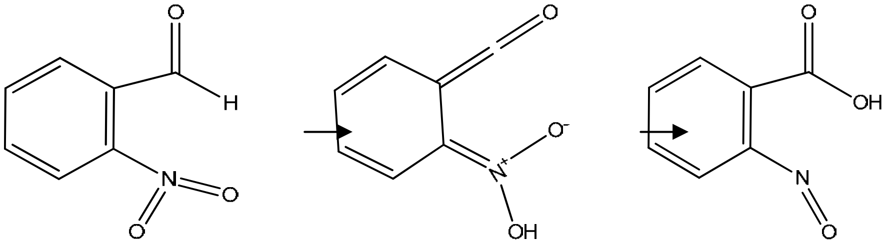

Figure 4.2: The photoacid is believed to undergo a ketene intermediate.

Before using the photoacid to trigger photochemical reactions, the mechanisms it undergoes itself must be understood in infrared spectroscopic terms. To do this, firstly an FTIR study was carried out. This allowed the photoacid to be understood in steady state, to determine the maximum concentrations available in the solvents used, also to help confirm absorption bands observed in spectra obtained later in TRIR measurements.

Results and discussion

The solvent initially used was 100% D_2O. This was to ensure the environment was consistent with experiments carried out later with the model poly-peptide. However, the solubility of the photo-acid in D_2O was poor. Therefore, methanol-D_4 was introduced and a ratio of the two solvents was used. Deuterated methanol was used as it increases the solubility of the photoacid and since it is deuterated, there will be no H-D exchange with D_2O which would result in the production of water in the sample and this would be observed in the FTIR spectrum, distorting the spectrum recorded for the sample. Ratios of 50-50% and 75-25%, in favour of methanol-D_4 were used; therefore the concentration of photoacid could be increased. The ratios described are by volume. The maximum photoacid concentration possible for a 50-50% solvent was 300mM, and for 75-25% solvent, the highest possible photoacid concentration was 1M. The solubility of the photoacid was further increased when using acetonitrile as the solvent, where a maximum photoacid concentration of 5M was achieved. Figure 4.3(a) shows steady state FTIR spectra for oNBA, dissolved in acetonitrile, before and after UV exposure. Difference spectra are shown in Figure 4.3(b) for different concentrations of oNBA in acetonitrile. These spectra were obtained by subtracting the spectrum before UV exposure from that taken after. It was found that 2M oNBA produced the largest change in the spectrum, as seen in Figure 4.3(b). The peak labelled 1703cm^{-1} is assigned to the loss of the aldehyde C=O stretch[46,95]. The bleaches located at 1346 and 1532cm^{-1} correspond to group stretching vibrations of NO_2. The transient peak at 1734cm^{-1} is assigned to the CO band of the carboxylic acid.

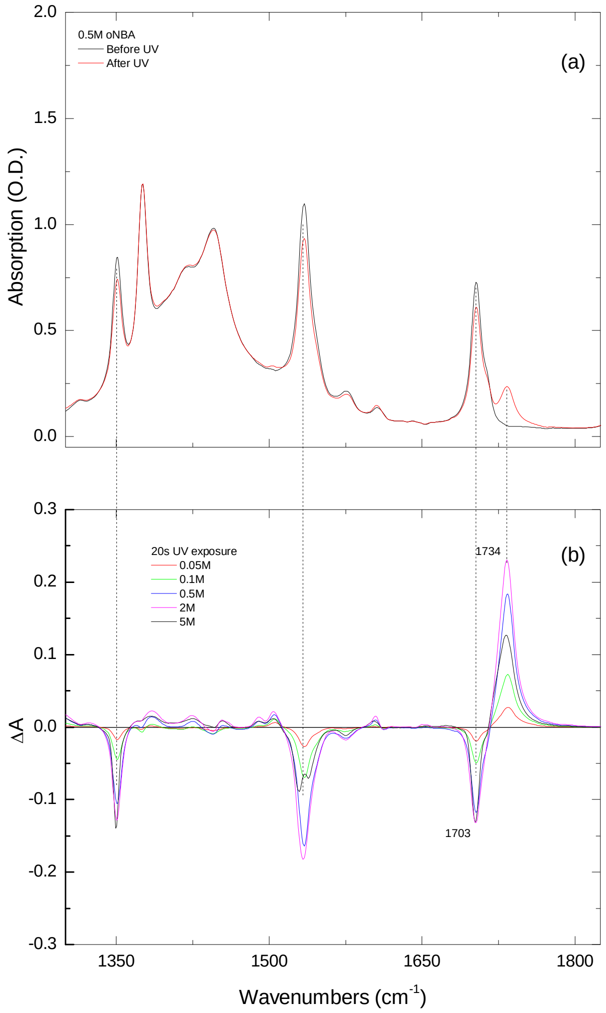

Figure 4.3: (a) Steady state FTIR for oNBA before and after UV exposure. (b) Difference Spectra showing concentration dependence on oNBA in acetonitrile.

Although using FTIR allows the initial and final conditions of the photoacid molecule to be determined, further analysis, with greater time resolution, would allow the change in the molecule throughout the course of the reaction to be understood. To do this, TRIR spectroscopy was employed to investigate the photoacid reaction in acetonitrile on a pico-second time scale. oNBA has been studied previously in acetonitrile using Raman spectroscopy.

TRIR spectroscopy was employed as well as FTIR for analysis of the photoacid. The set up and method for data treatment are described earlier in *Chapter 2 – Experimental Setup*. The photoacid was found to have an absorption band at 305nm, as shown in Figure 4.4, below. This absorption band corresponds to the photodissociation of the benzaldehyde[96]. When used with the hydrogenase enzymes, the UV pump pulse was tuned to 315nm, so that the photoacid could be excited without exciting the compounds $Fe_2(CO)_6$ and $Fe_2(CO)_4(PMe_3)_2$. After data treatment, the difference spectra shown in Figure 4.5 were obtained. Each spectrum is for a different time delay between the pump and probe beams. The time delays for the pump-probe beams were in the range of 1-500ps. By changing the time delays, it was possible to observe how the molecular structure changed and the time scale within which the changes occurred. When dissolved in a methanol-D_4/D_2O solvent mixture, the positions of the bleach and transient absorptions are shifted to a lower frequency by two or three wavenumbers, compared to the positions recorded in acetonitrile. The shift is attributed to hydrogen bonding, since it lowers stretching vibrations by lowering the restoring force[59].

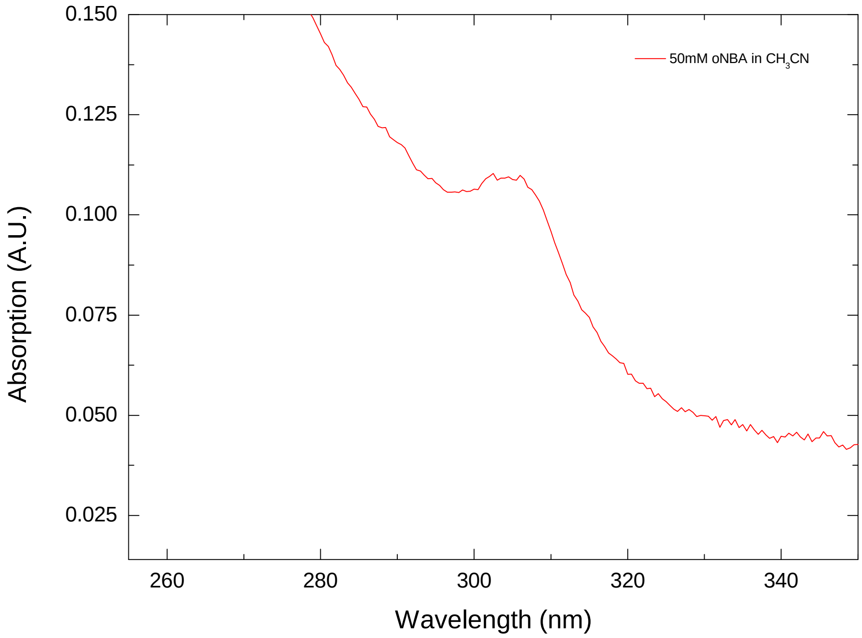

Figure 4.4: UV/Vis Spectrum of oNBA.

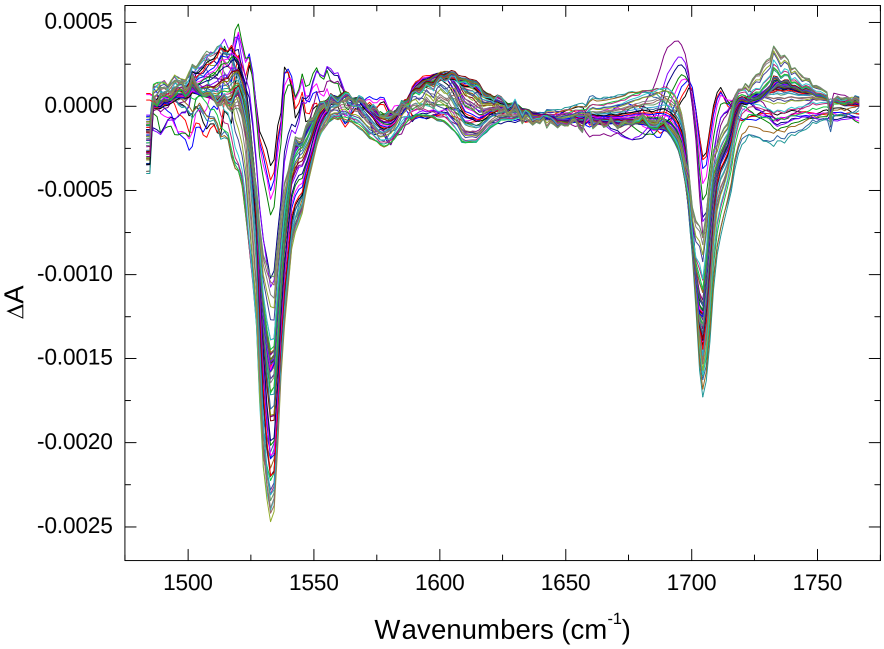

Figure 4.5: Pico-second TRIR of oNBA in acetonitrile.

By plotting the change in peak heights, which shows the change in absorption, kinetics can be obtained to determine the speed of change in the photoacid molecule. Figure 4.6 shows the kinetics for the 1532cm^{-1} NO_2 vibration and 1704cm^{-1}, the loss of the aldehyde CO vibration. Whilst using Gaussian functions to fit this data would provide information on the rate of change at any point on the data, it was sufficient to take only the size of the peaks of interest to analyse the kinetics of the peak.

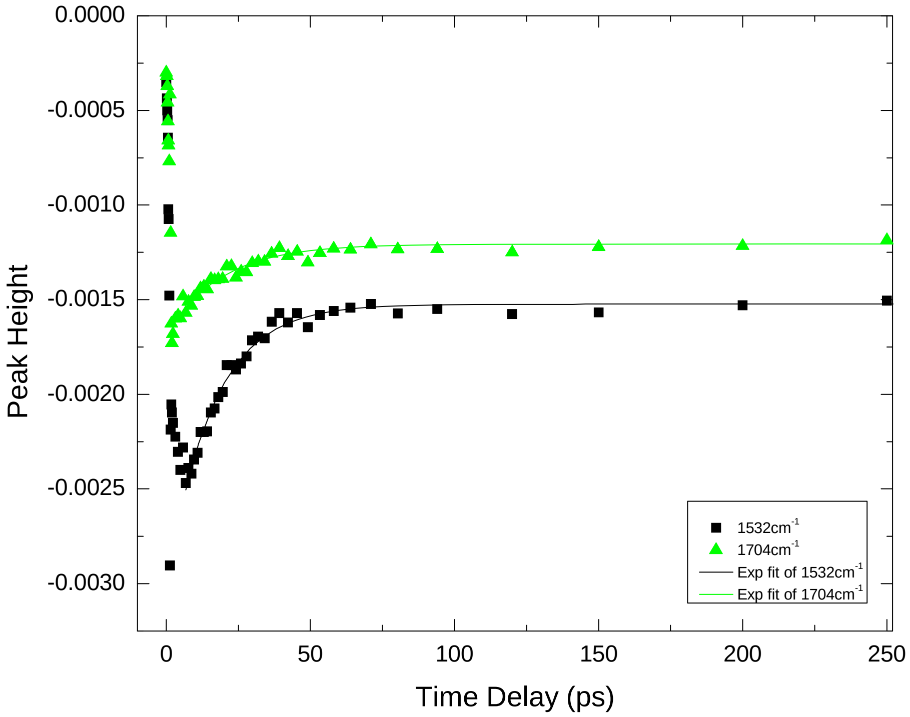

Figure 4.6: Change in peaks and exponential fits.

From Figure 4.6, it is clear that the dynamics for these peaks stop changing after 75ps. The data in the first two picoseconds corresponds to the instrument response time, from here on, it can be seen that the bleaches recovers, meaning there is a partial recovery of the mechanisms[46], which is due to a relaxation of electrons back to the ground state. The instrument response time corresponds to the length of the pulses i.e. at these very short delay times, the pump and probe pulses overlap. The 1532cm^{-1} peak has a recovery time of 15.5 ± 0.69ps and the 1704cm^{-1} has a recovery time of 19.19 ± 1.48ps. The data was acquired and averaged over four cycles. This explains why there is scatter in the data, which can be used to estimate errors.

The appearance of the carboxylic C=O stretch at ~1732cm^{-1} is not apparent in the data presented from the pico-second TRIR experiment. Therefore, a slower experiment, on the nanosecond scale was carried out to help identify the manifestation of the carboxylic content.

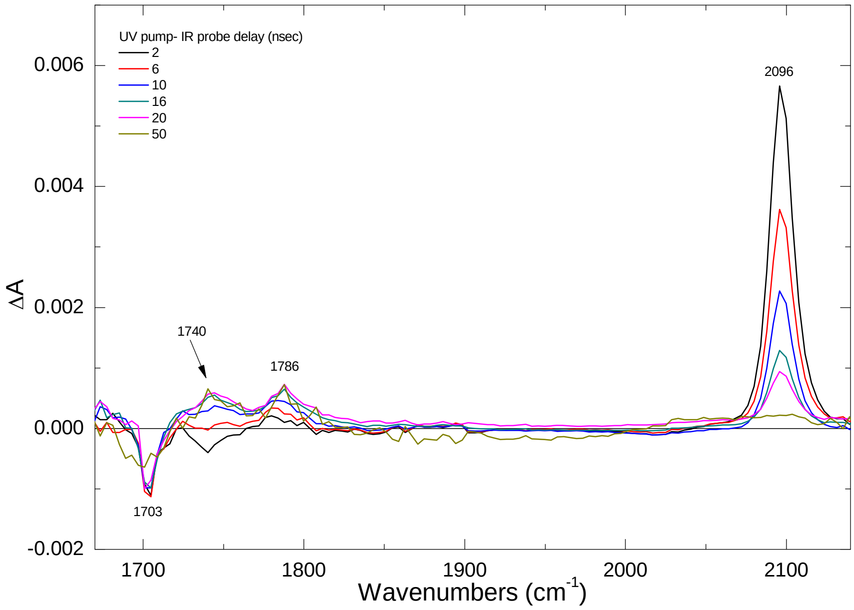

Figure 4.7: Nano-second TRIR showing the ketene intermediate of oNBA.

Upon further analysis of the main peaks in Figure 4.7, and fitting exponential functions to each, Figure 4.8 is produced. The peak associated with the ketene intermediate, at 2096cm^{-1} has a decay time of 8.44 ± 0.25ns. The 1740cm^{-1} peak has a rise time of 7.90 ± 0.69ns. The features at 1740cm^{-1} and 1786cm^{-1} are not clear in Figure 4.5 but are easily distinguished in the nano-second experiment.

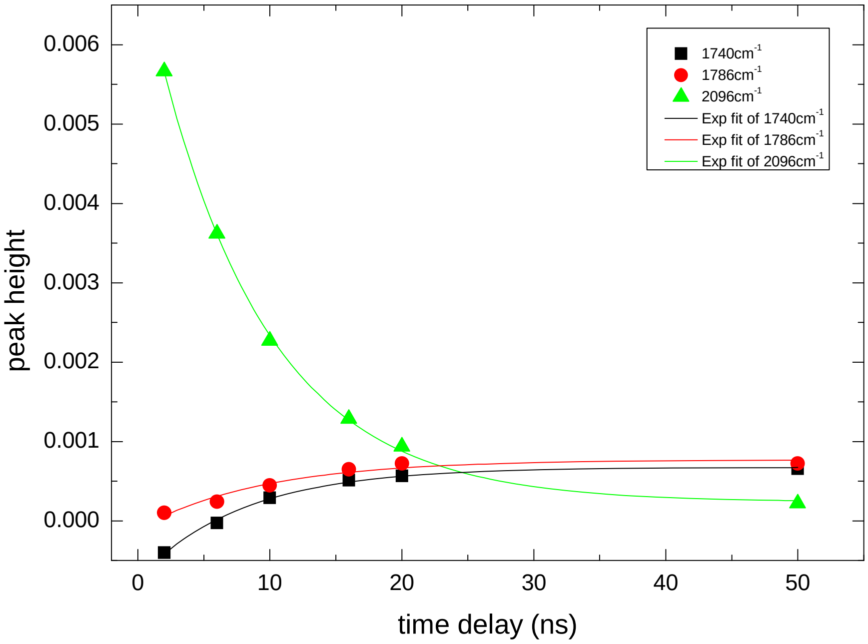

Figure 4.8: Change in peak height with exponential fits.

As the time delay is increased, it is clear that the ketene intermediate disappears. This is shown in Figure 4.8. The feature at 1786cm^{-1} appears on a slightly slower time scale, but is of the same order of magnitude as the ketene intermediate. It is clear that the 2096cm^{-1} peak falls as the 1740cm^{-1}, observed in the picosecond experiment, rises. The peak at 1740cm^{-1} associated with the acid has a rise time of 7.9 ± 0.69ns and is anti-correlated with the peak at 2096cm^{-1}, the ketene peak, which has a decay time of 8.44 ± 0.25ns. The mechanism occurs in two steps, where the rise time of the acid matches the decay time of the ketene peak within the band of the errors. This assignment of the ketene intermediate is consistent with that reported in the literature. It cannot be an overtone since overtones are too weak to be observed, in general.

Spectrum Position (cm^{-1})	Assignment	Reference
1346, 1532	Group stretching of NO_2	84
~1703	Loss of aldehyde CO	46,95
~1732 - 1740	Kinetic successor to ketene	46
2096	Ketene intermediate	44,46

Table 4.1: Assignments of oNBA Infrared absorptions and literature references.

Table 4.1 lists the important IR absorptions observed for oNBA, their assignments and reference to literature which record similar results. The photochemistry of oNBA has been studied for many years and can be examined using a variety of techniques. George and Scaiano[47] carried out a laser flash photolysis study which had nano second time resolution to observe the conversion of oNBA to nitrosobenzoic acid. They found that transients in the spectra were solvent dependent and had lifetimes in the range 50 to ≤ ~1ns. They report that these transients were associated with the triplet state of oNBA. However, Yip and Sharma[93] observed transients using pump-probe experiments of 35ps time resolution and assigned a 74ps transients to a ketene intermediate due to strong solvent dependencies, and the spectral signature obtained. They reported that the transient had a lifetime of 24 ± 8ns in acetonitrile. Femtosecond vibrational spectroscopy on the photochemistry of oNBA was performed by Laimgruber et al (2005)[44] who observed the ketene intermediate to have a lifetime of 13ps in a 1:1 mixture of ethanol:water solvent. The IR spectral position of this ketene intermediate was found to be 2100cm^{-1}, which is in good agreement with the data presented here. The lifetime for the ketene intermediate as presented here is 8.44 ± 0.25ns in acetonitrile. Laimgruber et al (2008)[45] reported a lifetime on the 10ns time scale for the lifetime of the ketene intermediate. The methods used here were femotsecond stimulated Raman spectroscopy (FSRS) as well as time dependent DTF calculations. It has been reported that the presence of water in a solvent significantly reduces the lifetime of the ketene intermediate[47,93].

The pH jump induced in this experiment can be estimated by approximating the conversion of aldehyde to acid. The initial aldehyde concentration was 0.5M. Taking the initial peak height from corresponding FTIR spectra at ~1703cm^{-1} and the final bleach height where there is a partial recovery of aldehyde, the maximum concentration of acid can be estimated to be 0.83mM. This is the concentration of un-dissociated acid, $[HA]$. Using the equation for K_a, Equation 4.1, the concentration of dissociated acid, A^- can be evaluated. For a weak acid, A^- and H^+ can be set equal to one another.

$$K_a = \frac{[A^-][H^+]}{[HA]} \qquad \text{Equation 4.1}$$

Using the K_a value for benzoic acid, 6.5x10^{-5}, $[A^-]$ is estimated to be 0.23mM. The value for pK_a is found to be 4.18 using Equation 4.2, below.

$$pK_a = -\log_{10} K_a \qquad \text{Equation 4.2}$$

Following on from this, the pH can be calculated using Equation 4.3;

$$pH = pK_a + \log\frac{[A^-]}{[HA]} \qquad \text{Equation 4.3}$$

The pH after conversion to acid is estimated to be pH 3.62. Assuming an initial pH of 7, this gives a pH jump of 3.38 pH units.

Once the mechanisms involved in the conversion of oNBA from a nitro to nitroso acid are understood, it can be applied to systems which make use of photo-initiated reactions. The pH of a model-polypeptide can be altered using the photoacid which in turn modifies the secondary structure, as will be discussed in the next section. The following section uses the photoacid to aid protonation of a hydrogenase system.

4.2 The Helix-To-Coil Transition Of Poly-L-Lysine

Introduction

The photoacid was used to induce a change in secondary structure in a model-polypeptide system. The helix-to-coil transition of poly-L-lysine is a well studied topic, however the use of a photoacid to trigger the transition is not well reported. IR Spectroscopy is used here to follow the transition, observed in the Amide I band region. The transition has been the subject of interest for many years and has been found to be dependent on solvent[97,98], temperature[99-101], pH[102] and a combination of pH and temperature i.e. changing temperature at extreme pH values[90]. The helix-to-coil transition of poly-L-lysine has been shown to influence the diffusion and permeability of membranes[103], where it has applications as a protein or drug carrier[104,105]. Lysine has a basic side chain, and so, is capable of accepting protons. Since oNBA is a proton donor, this makes the helix-to-coil transition of poly-L-lysine an interesting system to investigate using the photoacid. In solution, the initial secondary structure was observed to be random coil. Lysine contains the basic group, NH_2 and acidic group, COOH, as seen in Figure 4.9. An internal ion transfer between the two gives NH_3^+ and COO^-, resulting in an overall charge of zero. Increasing the pH of the model-polypeptide removes an ion from the NH_3^+ group. This causes the conformation of the polypeptide to change from coil to helix since the alpha helix is in the lowest energy state. In the helix-to-coil-transition, the helical conformation becomes protonated, leading to the charges on the side chains repelling each other meaning the alpha helix is less stable and the conformation converts to random coil. When dissolved in the photoacid, the transition is activated by exposing the sample to UV light. The changes were monitored using FTIR spectrum after exposing the sample to UV light.

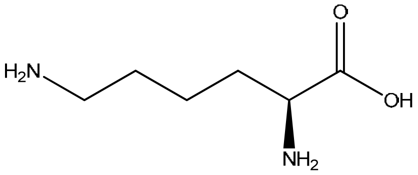

Figure 4.9: L-lysine.

The conformational transition of poly-L-lysine has been studied with changing temperature at stated pH values[102,104,106]. It has been studied using various techniques, including NMR spectroscopy, vibrational circular dichroism (VCD) and Raman spectroscopy. This study looks at the poly-peptide using FTIR spectroscopy. This will provide information on how the secondary structure changes as the pH changes. To initiate the change in structure, the photoacid is used, whereas in previous experiments, temperature was used at extreme pH values. The aim of the project is to recreate this helix-coil transition using the photoacid to simulate the denaturation process, because exposing the photoacid to UV light increases the $[H^+]$ concentration, decreasing the pH, which is what happens during denaturation.

Results and discussion

The pH of the sample was initially controlled by adding small (µl's) of NaOD solution (0.9M), sodium deuteroxide, a strong base. This meant the pH of the poly-peptide could be "tuned" and measured with a pH meter. Whilst the pH was measured, the samples were dissolved in deuterated solvent, therefore, a correction as described by Glasoe et al[107] to give pD was performed, as per Equation 4.3.

$$pD = pH_{measured} + 0.4 \qquad \text{Equation 4.3}$$

Figure 4.10 shows FTIR of the transition, left, and a titration plot of change in peak positions against the measured pH, right. A solution consisting of 1.5ml D_2O and 30mg poly-L-lysine was prepared to carry out this calibration experiment. FTIR spectra were obtained with 256 scans with a spectral resolution of 1.5cm^{-1}. A pathlength of 100µm was used in the sample cell. This graph was used as a calibration curve for future experiments to estimate the pH of the sample, by deducing where the helix-to-coil transition was occurring. It was used to determine that the pH jump-induced structural change occurred between pD9.9 and pD11.9. This is clearly a change in secondary structure, as the peak shifts from the characteristic position for random coil to that of alpha helix, due to protonation of the NH_2 side chain.

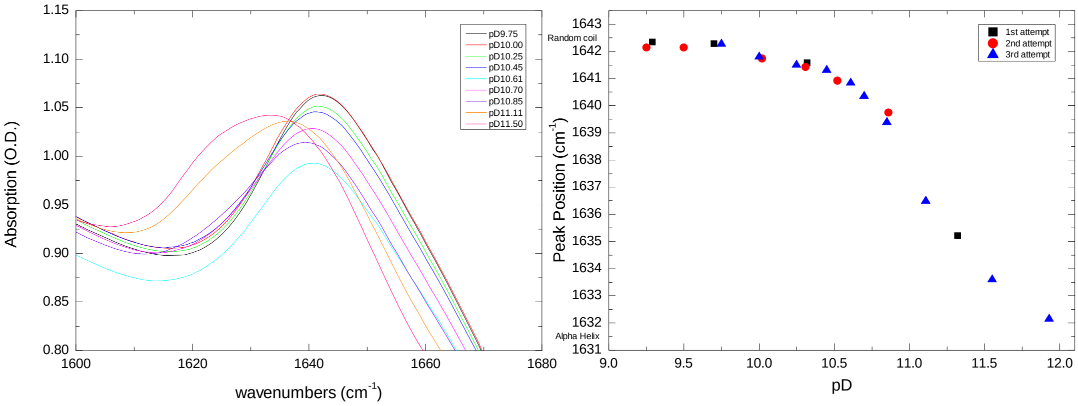

Figure 4.10: FTIR and the titration curve during “manual” pD change.

The initial pD of poly-L-lysine was calculated to be 9.75, with a peak position of ~1642cm^{-1} in the Amide I band. As the pD was increased using NaOD, the peak position shifted to lower wavenumbers. This implied the secondary structure changed from random coil to alpha helix when the pD was increased.

Once the pD range was established, the photoacid, oNBA, was used to induce the change in secondary structure. The concentrations of solvent were also varied, from 100% D_2O to 100% methanol-D_4. oNBA of 10mM was prepared, which was the highest concentration of oNBA that could be obtained in this solvent. Poly-L-lysine of 0.88mM was then added to the photoacid solution. The initial conformation of the sample was alpha helix. After exposure to UV light, the peak is shifted to higher wavenumbers, therefore assuming a random coil conformation. FTIR was collected before and after exposing the sample to UV light. A set time of 1 minute was given to expose the sample between FTIR measurements. This was found to be a sufficient length of time for exposure of the sample for the photoacid conversion. This exposure time was determined by carrying out various experiments using different exposure times.

The addition of NaOD, which has a high value of pH and therefore very basic, deprotonated the sample, leading to the side chains becoming uncharged. This led to the alpha helix conformation being the more favoured structure i.e. the presenting the lowest energy state. The aim is then to expose the sample to UV light, initiating the change in the photoacid, therefore protonating the sample inducing the change in secondary structure. It was found that by adding between 30 and 40µl of NaOD at a concentration of 0.89M produced the largest change in the spectrum, which is evident in Figure 4.11, which shows the difference spectra for 30mg poly-L-lysine in 10mM oNBA dissolved in a 50-50 solvent mixture.

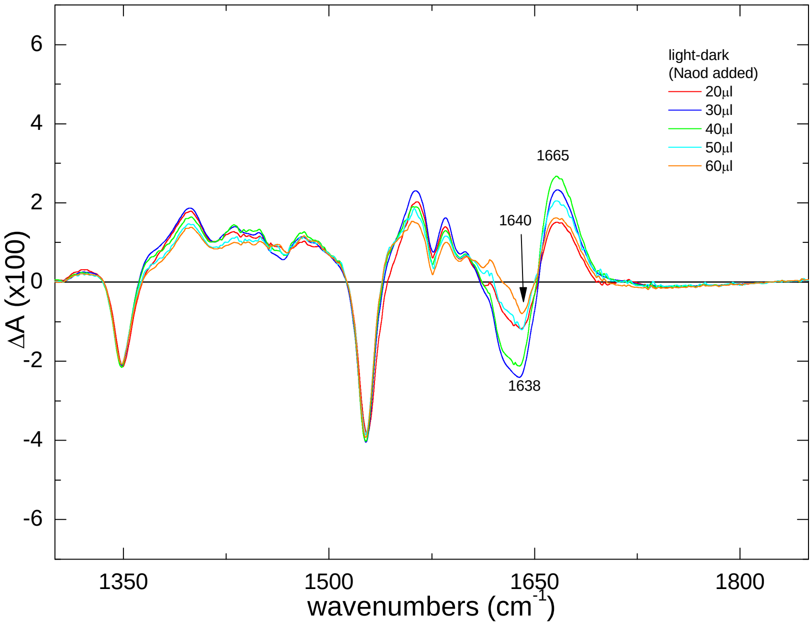

Figure 4.11: Difference spectra for poly-L-lysine in oNBA.

The spectra in Figure 4.11 were produced by subtracting the initial spectrum of poly-L-lysine dissolved in oNBA before exposure to UV light, from the resulting spectrum after it was exposed to UV light. This allows the changes in structure to be observed from the initial to final state of the sample. The changes in secondary structure are observed in the Amide I band region, from 1600 to 1700cm^{-1}. The bleach, which varies in position from 1638 to 1640cm^{-1} represents the loss of helix structure, and the transient peak at 1665cm^{-1} is the gain of random coil secondary structure, which is in agreement with past literature[102].

In 1965, Appel and Yang[97] conducted experiments to determine if the use of D_2O instead of H_2O had an effect on the structural shift. They found that it did not, and observed the titration of poly-L-lysine to be in the region of pD9-12, which is in good agreement with the data presented here. VCD was carried about by Yasui and Keiderling[102] to study the conformation of poly-L-lysine as a function of pH. They found that the random coil conformation occurred at neutral pH and found the VCD spectrum for this to be in agreement with past work. Where IR spectra showed an absorption in the Amide II band, VCD did not record a response. A small frequency shift between alpha helix and random coil is represented by a sign reversal in the VCD spectrum, whilst the change from alpha helix to beta-sheet was observed as a splitting of a band into two. A 2D Raman optical activity (ROA) study was carried out by Ashton et al[90] to observe the transition of poly-L-lysine from alpha helix to beta sheet. A temperature-dependent study using UV resonance Raman spectroscopy to examine beta formations of poly-L-lysine was also undertaken by JiJi et al[101]. As expected, the transition from alpha helix to beta-sheet occurs at high pH (pD). The conformational stability of the alpha helix at high pH is reduced. However, the transition to beta-sheet is triggered by an increase in temperature, where the alpha helical content undergoes 'thermal melting'. An isotope labelled solid state NMR study of the conformations of poly-L-lysine by Dos et al[104]. They observed that at high values of pH (>10), the spectra showed dramatic changes, which can be attributed to the conversion from alpha helix to beta-sheet. The purpose of isotopic labelling in such experiments is to provide a controlled point in the spectrum which is known to be the isotope.

With the use of 2DIR spectroscopy to follow the transition, a more comprehensive appreciation of the mechanisms within the transition will be gained. Line shape analysis would play an important role here, as secondary structure conformations have distinct patterns within both an FTIR and 2DIR spectrum.

4.3 [Fe-Fe] Hydrogenase Model Enzyme System

Introduction

The purpose of the hydrogenase model enzyme system is to catalyse a reversible oxidation of molecular hydrogen, as per the reaction $H_2 \leftrightarrow 2H^+ + 2e^-$. Understanding the chemistry of this reaction using the hydrogenase species is of significance since it could lead to new, cheaper materials for use in fuel cells[49,108]. These model systems consist of a di-metallic centre bridged by two Sulfur atoms. Six ligands are shared between a [Fe-Fe] centre. $Fe_2(CO)_6$ is the simplest form of the compound. Molecular hydrogen is produced via protonation of the [Fe-Fe] subsite[50]. This makes these hydrogenase systems ideal to study with the photoacid. These metal carbonyl compounds are structurally similar to the active sites of complex enzyme systems, and so, allows the active site to be studied without the complication of surrounding proteins, which buries the active site where the molecular hydrogen is created. The study of the vibrational relaxation mechanisms of the model active site will lead to determining the role of the surrounding protein scaffold[109]. Ultimately, this allows the active site and the protein to be investigated separately. The enzyme relies on the formation of a vacant coordination site on one of the Fe atoms[110]. The two compounds considered here are $Fe_2(CO)_6$ and $Fe_2(CO)_4(PMe_3)_2$ which are shown below in Figure 4.12.

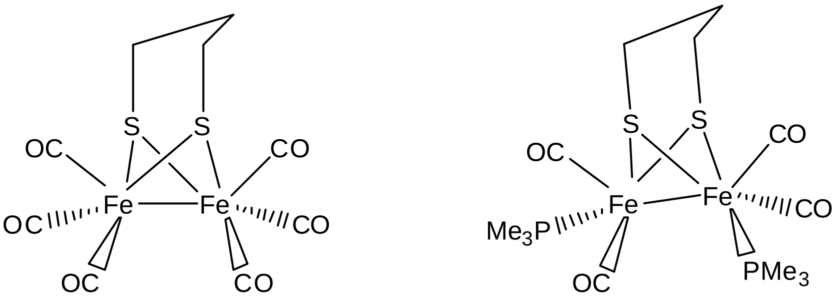

Figure 4.12: $Fe_2(CO)_6$ and $Fe_2(CO)_4(PMe_3)_2$.

Metal carbonyls offer a great deal of chemistry that can be studied with IR spectroscopy, obviously, carbonyl stretches. Previous work on metal carbonyls such as these has comprised 2DIR studies on $FE_2(CO)_6$ which provided information on structure and vibrational dynamics when dissolved in heptane[49], as well as probing it with a UV_{pump} – IR_{probe} transient 2DIR experiment to determine photoproducts of the compound upon photo-excitation[109]. This also offers the opportunity to determine information on the metal-to-ligand charge transfer and solvent interactions[111]. $Fe_2(CO)_4(PMe_3)_2$ has been studied using stopped-flow UV and IR spectroscopy, with a view to providing an understanding of the mechanisms in the protonation of the active site[50,51]. Fe-hydrogenase systems have been shown to be light sensitive[112], where there is evidence of an exchange between the ligands and Iron centre.

Measurements were carried out using an FTIR cell with KBr windows and a fixed pathlength of 50µm. For UV exposure, a xenon lamp with range 240-2000nm and output power of 75W was used. Samples had to be exposed for a longer time, typically 2 minutes, since the UV source has a low power output. While a concentration of 2M was found to be the optimum for oNBA in acetonitrile, a maximum of 0.5M could be used when the compounds were introduced. This was due to experimental limitations with equipment, which meant that if the maximum of 2M was used, the optical density of the sample in an IR experiment would be much higher than the acceptable standard, as described earlier in *Experimental Setup*. acetonitrile was used for consistency with previous work carried out in stopped-flow experiments[50,51].

Results and discussion

FTIR were obtained of $Fe_2(CO)_6$ and oNBA to use as reference spectra before continuing with more experiments to vary the conditions of the experiment. A 200mM sample of oNBA was prepared in acetonitrile. 2mM $Fe_2(CO)_6$ was also dissolved in acetonitrile. 1ml from each was mixed together and Figure 4.13 shows the raw FTIR spectra for both $Fe_2(CO)_6$ and oNBA and the mixture of the two. The effective concentrations are halved when the mixture of compound and photoacid is made, and so it can be seen in Figure 4.13 that the relative heights of both the photoacid and hydrogenase peaks are halved when the FTIR of the mixture is taken. It is clear to identify which peaks are due to the photoacid and which are due to the compound; the black spectrum shows oNBA only and the red shows $Fe_2(CO)_6$ only. When both the photoacid and the compound are in the sample, the resulting spectrum is shown in blue. The peaks between 1950 and 2100cm^{-1} correspond to group vibrations of $(CO)_6$.

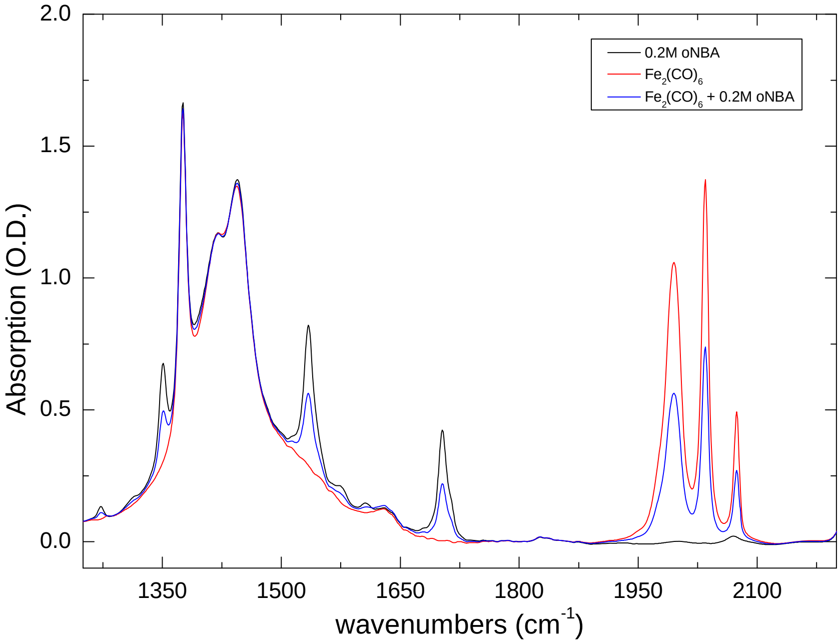

Figure 4.13: Raw FTIR for oNBA, $Fe_2(CO)_6$ and mixture.

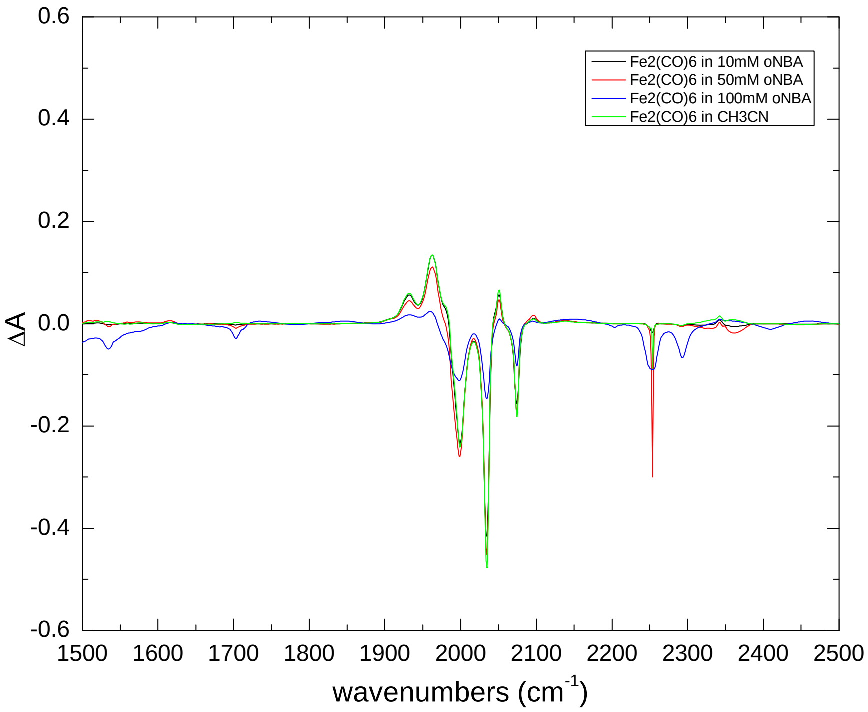

Figure 4.14: Comparison of $Fe_2(CO)_6$ in different concentrations of oNBA.

The difference spectra shown in Figure 4.14, above, are created by subtracting the spectrum after UV illumination from the spectrum before. It shows a difference spectrum of the hexacarbonyl dissolved in different concentrations of oNBA and also dissolved in acetonitrile only. The positions of the negative (bleach) peaks are in agreement with 2DIR experiments carried out and correspond to the ground state carbonyl stretching modes due to stimulate emission[49]. 2074cm^{-1} is attributed to the symmetric stretch of $(CO)_6$ whilst 2033cm^{-1} is assigned to the asymmetric stretch of $(CO)_3FeFe(CO)_3$. The transient absorptions located at 1932, 1963 and 2051cm^{-1} are also in agreement with experiments previously conducted on the compound[110]. These transients can be assigned to the formation of a solvent adduct. This is when the solvent interacts with the compound, where a CO ligand is dissociated and a solvent molecule coordinates in the free site. Solvent displacement is due to the changes in strength of the hydrogen bonds to the carbonyl ligands[49,109]. There is a small transient peak at 2096cm^{-1} which may be related to the ketene intermediate of the photoacid, since it is in the characteristic position for this. Protonation of the compound was not evident in this experiment, as it was suspected the photoacid and compound were not interacting to form a photoproduct.

Stopped-flow IR spectroscopic measurements have already been carried out on $Fe_2(CO)_4(PMe_3)_2$ to determine the mechanisms involved in protonation of the compound[51]. Stopped-flow spectroscopy is a technique which is used for rapid mixing of solutions and can produce kinetics of a reaction in solution. Whilst this is a good technique to observe reactions like those here, the use of TRIR can ultimately provide faster kinetics because the stopped-flow technique works on the order of milli-seconds. The time resolution of this technique is limited by the mixing procedure at the start of the experiment. With TRIR or 2DIR, it is possible to observe the reaction on nano- or pico-second time scales.

As with the hexacarbonyl, FTIR studies with varying oNBA concentration were carried out on this compound. Carrying out the same reaction but using the photoacid, the starting point of the reaction can be controlled thanks to the photo-activation of the photoacid. The data gathered from the stopped-flow experiment can be used to compare with that gathered via steady state FTIR. Figure 4.15 shows the raw spectra for the compound, the photoacid and the mixture of both.

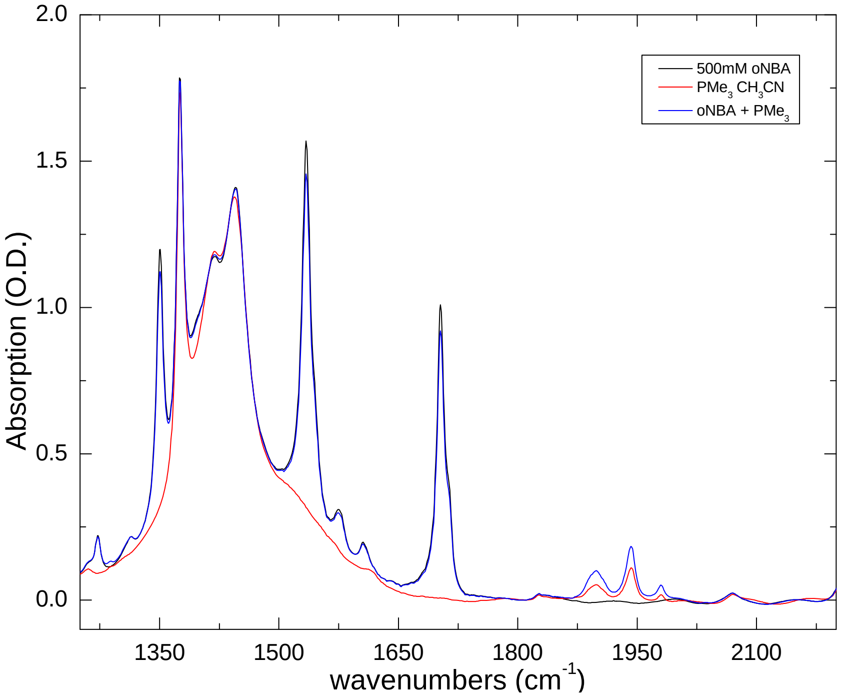

Figure 4.15: Raw spectra for oNBA, compound PMe$_3$ and the mixture of the two.

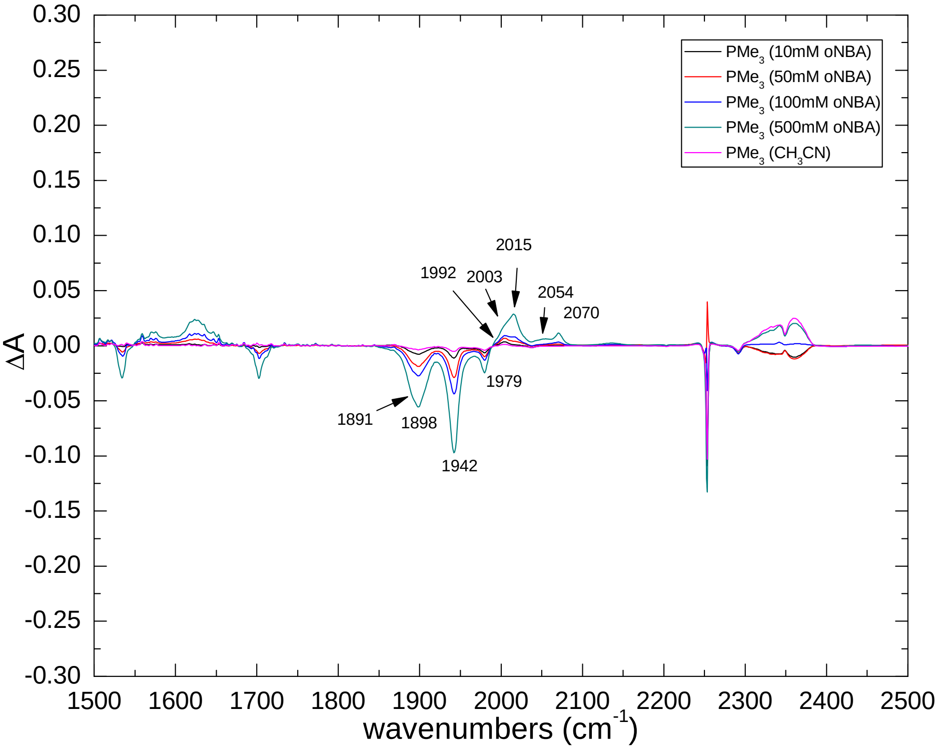

Figure 4.16: Difference Spectra for PMe$_3$ and oNBA at different concentrations.

Figure 4.16 shows the compound, $FE_2(CO)_4(PMe_3)_2$, dissolved in acetonitrile at different concentrations of photoacid. The bleaches labelled are assigned to the loss of the starting material of the compound, and the transient peaks at higher frequencies can be assigned to a photoproduct of the compound and the photoacid, which suggests that protonation is taking place.

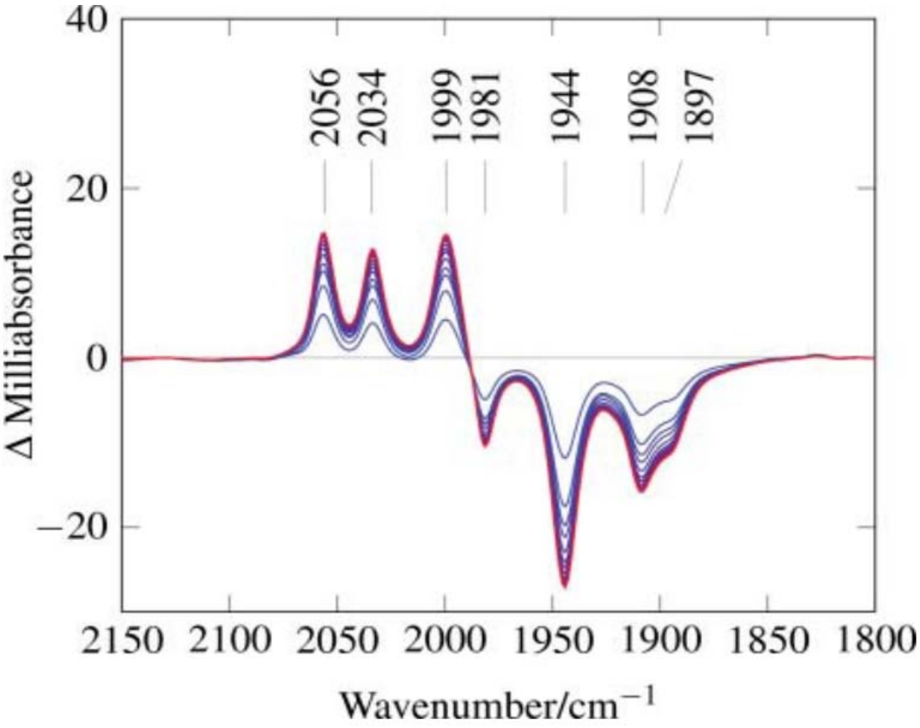

Figure 4.17[vi]: Difference spectra for PMe_3 as carried out using the stopped-flow technique[51].

Figure 4.17 shows the data gathered in previous stopped-flow experiments. Bleaching peaks in the stopped-flow spectra are attributed to the loss of the starting material due to protonation, which is assigned to the transient peaks[51]. Due to personal preference, the frequency axis in Figure 4.17 is reversed. Whilst both the FTIR and stopped-flow experiments show evidence for protonation, the absorption positions are not the same in both. This is detailed in Table 4.2, which shows the positions for both transients and bleaches in the FTIR and stopped-flow experiments.

[vi] Graph taken from: (51) Jablonskytė, A.; Wright, J. A.; Pickett, C. J. *Dalton Transactions* **2010**, *39*, 3026.

Bleaches		Transients	
FTIR	Stopped-Flow	FTIR	Stopped-Flow
1891	1897	1992	1999
1898	1908	2003	2034
1942	1944	2015	2056
1979	1981	2054	
		2070	

Table 4.2: Comparison of bleaches and transients for FTIR and stopped-flow experiments.

There are additional peaks at lower frequencies in the photo-activated experiment, which as before, in the hexacarbonyl measurements, suggests the loss of CO content. Peaks above 2000cm^{-1} correspond to protonation of the compound, since the bonds will vibrate with a higher frequency. This is clear in Figure 4.17, and is evident on Figure 4.16, but there are also photoproducts observed where the photoacid has coordinated with the compound. The concentration of the compound in the stopped-flow experiment is a fraction of that used in the FTIR experiment. Solvents were consistent between both experiments. In the stopped-flow experiment, $HBF_4 \cdot Et_2O$ was used to dissolve the compound. HBF_4 is a very strong acid, whereas oNBA is a weak acid. These differences may contribute to the disagreeing peak positions described in Table 4.2. The peak found at 2070cm^{-1} may be related to the ketene intermediate of oNBA[46]. It is unlikely to be an overtone band since the spectral position is not high enough to correspond to an overtone from vibrations in the molecule and is also not significantly smaller than other bands in the spectrum.

Conclusions

The data presented here for the photoacid, oNBA, shows that there is an intermediate step in the photoreaction which sees it transform from NBA to nitrosobenzoic acid is depicted in Figure 4.2. It is thought that the transformation of oNBA to o-nitrosobenzoic acid undergoes a transfer of hydrogen from the aldehyde to the nitro group, resulting in a ketene intermediate[44,46,47,93]. Initial FTIR data shows the initial and final states of the photoacid. In order to investigate the intermediate, TRIR spectroscopy had to be employed, which offered an insight into the intermediate states in the reaction. The initial loss of the aldehyde was observed at 1703cm^{-1}, as observed in both FTIR and TRIR spectra. Pico-second TRIR did not observe the gain of the carboxylic acid, and so a relatively slower (nano-second) experiment was needed. This showed that at short pump-probe delays there was a transient peak centred at 2096cm^{-1}. This peak is assigned to the ketene intermediate. As the time delay between the pump and probe was increased, this transient was found to decrease to zero. At the same time, the peak assigned to the final carboxylic acid content of the photoacid appeared with similar kinetics as the decreasing ketene peak, as shown in Figure 4.7.

The photoacid was used to trigger the helix-to-coil transition of the model poly-peptide, poly-L-lysine. The poly-peptide was found to assume an alpha helix conformation at high values of pH. The photoacid was introduced and by exposing the sample to UV light, triggering the photoacid in its own reaction, which sees the concentration of [H^+] increased, and according to the relation, $pH = -log[H^+]$, decreases the pH of the sample. This leads to the denaturation of the polypeptide, which alters the conformation it.

Protonation of the model hydrogenase enzyme systems was carried out through exposure to UV light when dissolved in the photoacid, oNBA. Two compounds were considered here, $Fe_2(CO)_6$ and $Fe_2(CO)_4(PMe_3)_2$. The protonation of $FE_2(CO)_6$ was not evident through FTIR analysis, but protonation of $Fe_2(CO)_4(PMe_3)_2$ was observed. By altering the concentration of the photoacid, it was possible to examine the amount of protonation of the sample, as evident in the difference spectra presented.

Chapter 5: Conclusions

Steady state FTIR and TRIR spectroscopy have been used successfully to study the interactions occurring in peptide and enzyme systems. The self-assembly of a peptide was studied and mechanisms of π-π interactions and the formation of beta-sheets was observed. It was found that π-stacking of the fluorenyl groups occurred before the formation of secondary structure beta-sheets.

The mechanisms undertaken by the photoacid, oNBA, upon UV excitation was considered and then applied to two different systems. It was found that there is an intermediate molecular structure in the photo-reaction. The data presented suggests this intermediate occurs on a time scale of the order of nano-seconds after the reaction is triggered. The disappearance of this intermediate, believed to be ketene, can be anti-correlated with the appearance of the final nitroso structure of the photoacid, since analysis shows that the rise time of one and the decay rate of the other are very close within the bounds of errors.

The first application of oNBA as a photo-trigger is a pH-jump induced secondary structure transition in a model poly-peptide, which simulates the process of denaturation. The process was replicated by first increasing the overall pH (pD) of the sample which encourages the poly-peptide to assume an alpha-helix conformation by changing the charge on the side chains. Upon UV excitation, oNBA undergoes its reaction, producing [H^+], decreasing the pH and therefore causing the poly-peptide to denature.

The second was a hydrogenase enzyme system which was observed to undergo protonation upon UV exposure when the photoacid was present. Two compounds were considered, both with di-iron centred hydrogenase. Data obtained on the $Fe_2(CO)_6$ compound were in agreement with previous experiments which showed transient absorptions corresponding to a solvent adduct, where the solvent molecules interact with the compound, and the bleaches observed match with prior experiments which assign these beaches to (CO) stretches of the compound.

Experiments carried out on $Fe_2(CO)_4(PMe_3)_2$ showed that a comparison between stopped-flow experiments and the data presented here do not agree. This may be because of solvent adducts or interactions with the photoacid.

These systems are ideal candidates for 2DIR spectroscopy as they involve fast interactions which are observable thanks to the good time resolution that can be obtained and the information that can be interpreted from the spectra; vibrational coupling and population transfer being the main reasons. The good time resolution also allows for kinetics to be attained over very short time scales.

References

(1) Barth, A.; Zscherp, C. *Quarterly Reviews of Biophysics* **2002**, *35*, 369.

(2) Selkoe, D. J. *Nature* **2003**, *426*, 900.

(3) Dobson, C. M. *Nature* **2003**, *426*, 884.

(4) Kolano, C.; Helbing, J.; Kozinski, M.; Sander, W.; Hamm, P. *Nature* **2006**, *444*, 469.

(5) Gunaratne, T. C.; Milliken, M.; Challa, J. R.; Simpson, M. C. *Applied Optics* **2006**, *45*, 558.

(6) Benabbas, A.; Ye, X.; Kubo, M.; Zhang, Z. Y.; Maes, E. M.; Montfort, W. R.; Champion, P. M. *Journal of the American Chemical Society* **2010**, *132*, 2811.

(7) Kim, Y. S.; Hochstrasser, R. M. *The Journal of Physical Chemistry B* **2009**, *113*, 8231.

(8) van der Spoel, D.; Marklund, E. G.; Larsson, D. S. D.; Caleman, C. *Macromolecular Bioscience* **2010**, *11*, 50.

(9) Kim, Y. S.; Hochstrasser, R. M. *Proceedings of the National Academy of Sciences of the United States of America* **2005**, *102*, 11185.

(10) van Thor, J. J. *Chem Soc Rev* **2009**, *38*, 2935.

(11) Onufriev, A.; Case, D. A.; Ullmann, G. M. *Biochemistry* **2001**, *40*, 3413.

(12) Kumar, D. P.; Tiwari, A.; Bhat, R. *Journal of Biological Chemistry* **2004**, *279*, 32093.

(13) Skinner, A. L.; Laurence, J. S. *Journal of Pharmaceutical Sciences* **2008**, *97*, 4670.

(14) Un, S.; Dorlet, P.; Rutherford, A. W. *Applied Magnetic Resonance* **2001**, *21*, 341.

(15) Mobius, K.; Savitsky, A.; Schnegg, A.; Plato, M.; Fuchs, M. *Physical Chemistry Chemical Physics* **2005**, *7*, 19.

(16) Yasui, S. C.; Keiderling, T. A. *Journal of the American Chemical Society* **2002**, *108*, 5576.

(17) Sreerama, N.; Woody, R. W. *Protein Science* **2004**, *13*, 100.

(18) Ranjbar, B.; Gill, P. *Chemical Biology & Drug Design* **2009**, *74*, 101.

(19) Catanzano, F.; Gambuti, A.; Graziano, G.; Barone, G. *Journal of Biochemistry* **1997**, *121*, 568.

(20) Kubelka, J.; Chiu, T. K.; Davies, D. R.; Eaton, W. A.; Hofrichter, J. *Journal of Molecular Biology* **2006**, *359*, 546.

(21) Rosenheck, K.; Doty, P. *Proceedings of the National Academy of Sciences of the United States of America* **1961**, *47*, 1775.

(22) Ling, Y. L.; Strasfeld, D. B.; Shim, S. H.; Raleigh, D. P.; Zanni, M. T. *Journal of Physical Chemistry B* **2009**, *113*, 2498.

(23) Clayden, J.; Greeves, N.; Warren, S.; Wothers, P. *OUP Oxford* **2000**, *ISBN: 0198503466*.

(24) Felli, I. C.; Brutscher, B. *Chemphyschem* **2009**, *10*, 1356.

(25) Berera, R.; van Grondelle, R.; Kennis, J. T. M. *Photosynthesis Research* **2009**, *101*, 105.

(26) Bell, S. E. J. *Analyst* **1996**, *121*.

(27) Frontiera, R. R.; Fang, C.; Dasgupta, J.; Mathies, R. A. *Physical Chemistry Chemical Physics*, *14*, 405.

(28) Frontiera, R. R.; Mathies, R. A. *Laser & Photonics Reviews*, *5*, 102.

(29) Williams, S.; Causgrove, T. P.; Gilmanshin, R.; Fang, K. S.; Callender, R. H.; Woodruff, W. H.; Dyer, R. B. *Biochemistry* **1996**, *35*, 691.

(30) Ganim, Z.; Sung, H.; Smith, A. W.; Deflores, L. P.; Jones, K. C.; Tokmakoff, A. *Accounts of Chemical Research* **2007**, *41*, 432.

(31) Marechal, A.; Ingledew, W. J.; Rich, P. R. *Biochemical Society Transactions* **2008**, *36*, 1165.

(32) Hill, J. R.; Dlott, D. D.; Rella, C. W.; Smith, T. I.; Schwettman, H. A.; Peterson, K. A.; Kwok, A.; Rector, K. D.; Fayer, M. D. *Biospectroscopy* **1996**, *2*, 277.

(33) Whitesides, G. M.; Mathias, J. P.; Seto, C. T. *Science* **1991**, *254*, 1312.

(34) Langer, R.; Tirrell, D. A. *Nature* **2004**, *428*, 487.

(35) Kokkoli, E.; Mardilovich, A.; Wedekind, A.; Rexeisen, E. L.; Garg, A.; Craig, J. A. *Soft Matter* **2006**, *2*, 1015.

(36) Jayawarna, V.; Ali, M.; Jowitt, T. A.; Miller, A. E.; Saiani, A.; Gough, J. E.; Ulijn, R. V. *Advanced Materials* **2006**, *18*, 611.

(37) Zhang, S. *Nat Nano* **2006**, *1*, 169.

(38) Smith, A. M.; Williams, R. J.; Tong, C.; Coppo, P.; Collins, R. F.; Turner, M. L.; Saiani, A.; Ulijn, R. *Advanced Materials* **2008**, *20*, 37.

(39) Das, A. K.; Collins, R.; Ulijn, R. V. *Small* **2008**, *4*, 279.

(40) Ulijn, R. V.; Smith, A. M. *Chemical Society Reviews* **2008**, *37*, 664.

(41) Strasfeld, D. B.; Ling, Y. L.; Gupta, R.; Raleigh, D. P.; Zanni, M. T. *Journal of Physical Chemistry B* **2009**, *113*, 15679.

(42) Avidan-Shpalter, C.; Gazit, E. *Amyloid-Journal of Protein Folding Disorders* **2006**, *13*, 216.

(43) Scherzinger, E.; Sittler, A.; Schweiger, K.; Heiser, V.; Lurz, R.; Hasenbank, R.; Bates, G. P.; Lehrach, H.; Wanker, E. E. *Proceedings of the National Academy of Sciences of the United States of America* **1999**, *96*, 4604.

(44) Laimgruber, S.; Schreier, W. J.; Schrader, T.; Koller, F.; Zinth, W.; Gilch, P. *Angewandte Chemie International Edition* **2005**, *44*, 7901.

(45) Laimgruber, S.; Schmierer, T.; Gilch, P.; Kiewisch, K.; Neugebauer, J. *Physical Chemistry Chemical Physics* **2008**, *10*, 3872.

(46) Schmierer, T.; Schreier, W. J.; Koller, F. O.; Schrader, T. E.; Gilch, P. *Physical Chemistry Chemical Physics* **2009**, *11*, 11596.

(47) George, M. V.; Scaiano, J. C. *Journal of Physical Chemistry* **1980**, *84*, 492.

(48) Osterhout, J. J.; Muthukrishnan, K.; Nall, B. T. *Biochemistry* **1985**, *24*, 6680.

(49) Stewart, A. I.; Clark, I. P.; Towrie, M.; Ibrahim, S. K.; Parker, A. W.; Pickett, C. J.; Hunt, N. T. *The Journal of Physical Chemistry B* **2008**, *112*, 10023.

(50) Wright, J. A.; Pickett, C. J. *Chemical Communications* **2009**, 5719.

(51) Jablonskytė, A.; Wright, J. A.; Pickett, C. J. *Dalton Transactions* **2010**, *39*, 3026.

(52) Bandekar, J.; Krimm, S. *Proceedings of the National Academy of Sciences of the United States of America* **1979**, *76*, 774.

(53) Reisdorf, W. C. J.; Krimm, S. *Biochemistry* **1996**, *35*, 1383.

(54) Cai, S.; Singh, B. R. *Biophysical Chemistry* **1999**, *80*, 7.

(55) Huan, J.; Prins, J.; Wang, W.; Chau-Wen, T. Local Structure Comparison of Proteins. In *Advances in Computers*; Elsevier, 2006; Vol. Volume 68; pp 177.

(56) Sewald, N.; Jakubke, H.-D. *Wiley-VCH Verlag GmbH, D-69469 Weinheim* **2002**.

(57) Ho, B. K.; Curmi, P. M. G. *Journal of Molecular Biology* **2002**, *317*, 291.

(58) DeFlores, L. P.; Ganim, Z.; Nicodemus, R. A.; Tokmakoff, A. *Journal of the American Chemical Society* **2009**, *131*, 3385.

(59) Barth, A. *Biochimica et Biophysica Acta (BBA) - Bioenergetics* **2007**, *1767*, 1073.

(60) Torii, H.; Tasumi, M. *Journal of Chemical Physics* **1991**, *96*, 3379.

(61) Asplund, M. C.; Zanni, M. T.; Hochstrasser, R. M. *Proceedings of the National Academy of Sciences of the United States of America* **2000**, *97*, 8219.

(62) Zanni, M. T.; Hochstrasser, R. M. *Current Opinion in Structural Biology* **2001**, *11*, 516.

(63) Park, S.; Kwak, K.; Fayer, M. D. *Laser Physics Letters* **2007**, *4*, 704.

(64) Bredenbeck, J.; Helbing, J.; Kolano, C.; Hamm, P. *ChemPhysChem* **2007**, *8*, 1747.

(65) Hunt, N. T. *Chemical Society Reviews* **2009**, *38*, 1837.

(66) Barth, A. *Progress in Biophysics & Molecular Biology* **2000**, *74*, 141.

(67) Morse, P. M. *Physical Review* **1929**, *34*, 57.

(68) Moore, J. H.; Spencer, N. D. *"Encyclopedia of Chemical Physics and Physical Chemistry" Volumes 1-3, I.o.P. Publication* **2001**.

(69) Zuev, V. E.; Ponomarev, Y. N.; Tikhomirov, B. A. *Optics Letters* **1984**, *9*, 490.

(70) Bratos, S.; Leicknam, J. C. *Journal of Chemical Physics* **1994**, *101*, 4536.

(71) Wynne, K.; Hochstrasser, R. M. *Chemical Physics* **1995**, *193*, 211.

(72) Strasfeld, D. B.; Ling, Y. L.; Shim, S. H.; Zanni, M. T. *Journal of the American Chemical Society* **2008**, *130*, 6698.

(73) Zheng, J.; Jang, H.; Ma, B.; Nussinov, R. *Journal of Physical Chemistry B* **2008**, *112*, 6856.

(74) Kyle, S.; Aggeli, A.; Ingham, E.; McPherson, M. J. *Biomaterials* **2010**, *31*, 9395.

(75) Silva, G. A.; Czeisler, C.; Niece, K. L.; Beniash, E.; Harrington, D. A.; Kessler, J. A.; Stupp, S. I. *Science* **2004**, *303*, 1352.

(76) Lost, R. M.; Crespilho, F. N. *Biosensors & bioelectronics* **2012**, *31*, 1.

(77) He, Q.; Cui, Y.; Ai, S.; Tian, Y.; Li, J. *Current Opinion in Colloid & Interface Science* **2009**, *14*, 115.

(78) Aggeli, A.; Bell, M.; Carrick, L. M.; Fishwick, C. W. G.; Harding, R.; Mawer, P. J.; Radford, S. E.; Strong, A. E.; Boden, N. *Journal of the American Chemical Society* **2003**, *125*, 9619.

(79) Chi, X.; Guerin, A. J.; Haycock, R. A.; Hunter, C. A.; Sarson, L. D. *Journal of the Chemical Society, Chemical Communications* **1995**, 2563.

(80) Williams, R. J.; Smith, A. M.; Collins, R.; Hodson, N.; Das, A. K.; Ulijn, R. V. *Nature Nanotechnology* **2009**, *4*, 19.

(81) Ercolani, G. *Journal of Physical Chemistry B* **2003**, *107*, 5052.

(82) Das, A. K.; Hirst, A. R.; Ulijn, R. V. *Faraday Discussions* **2009**, *143*, 293.

(83) Berthomieu, C.; Hienerwadel, R. *Photosynthesis research* **2009**, *101*, 157.

(84) Lin-Vien, D.; Colthup, N. B.; Fateley, W. G.; Grasselli, J. G. *Academic Press, San Diego, California 92101* **1991**.

(85) Cheatum, C. M.; Tokmakoff, A.; Knoester, J. *Journal of Chemical Physics* **2004**, *120*, 8201.

(86) Demirdoven, N.; Cheatum, C. M.; Chung, H. S.; Khalil, M.; Knoester, J.; A.Tokmakoff. *Journal of the American Chemical Society* **2004**, *126*, 7981.

(87) Yagai, S.; Karatsu, T.; Kitamura, A. *Chemistry-a European Journal* **2005**, *11*, 4054.

(88) Martinez, M. J.; Farias, M. E.; Pilosof, A. M. R. *Food Hydrocolloids*, *25*, 860.

(89) Loveday, S. M.; Wang, X. L.; Rao, M. A.; Anema, S. G.; Singh, H. *Journal of Agricultural and Food Chemistry*, *59*, 8467.

(90) Ashton, L.; Barron, L. D.; Czarnik-Matusewicz, B.; Hecht, L.; Hyde, J.; Blanch, E. W. *Molecular Physics: An International Journal at the Interface Between Chemistry and Physics* **2006**, *104*, 1429

(91) Bowen, E. J.; Hartley, H.; Scott, W. D.; Watts, H. G. *Journal of the Chemical Society, Transactions* **1924**, *125*, 1218.

(92) Leighton, P. A.; Lucy, F. A. *J. Chem. Phys.* **1934**, *2*, 756.

(93) Yip, R.; Sharma, D. *Research on Chemical Intermediates* **1989**, *11*, 109.

(94) Cheng, S.; Song, P.; Yang, S.; Yin, H.; Han, K. *Physical Chemistry Chemical Physics* **2010**, *12*.

(95) Causgrove, T. P.; Dyer, R. B. *Chemical Physics* **2006**, *323*, 2.

(96) Zhu, L.; Cronin, T. J. *Chemical Physics Letters* **2000**, *317*, 227.

(97) Appel, P.; Yang, J. T. *Biochemistry* **1965**, *4*, 1244.

(98) Susi, H.; Timasheff, S. N.; Stevens, L. *The Journal of biological chemistry* **1967**, *242*, 5460.

(99) Davidson, B.; Fasman, G. D. *Biochemistry* **1967**, *6*, 1616.

(100) Muller, M.; Buchet, R.; Fringeli, U. P. *Journal of Physical Chemistry* **1996**, *100*, 10810.

(101) JiJi, R. D.; Balakrishnan, G.; Hu, Y.; Spiro, T. G. *Biochemistry* **2006**, *45*, 34.

(102) Yasui, S. C.; Keiderling, T. A. *Journal of the American Chemical Society* **1986**, *108*, 5576.

(103) Sjögren, H.; Ulvenlund, S. *Biophysical Chemistry* **2005**, *116*, 11.

(104) Dos, A.; Schimming, V.; Chan-Huot, M.; Limbach, H. *Physical Chemistry Chemical Physics* **2010**, *12*, 10235.

(105) Shen, W. C.; Ryser, H. J. P. *Proceedings of the National Academy of Sciences of the United States of America-Biological Sciences* **1981**, *78*, 7589.

(106) Dzwolak, W.; Ravindra, R.; Nicolini, C.; Jansen, R.; Winter, R. *Journal of the American Chemical Society* **2004**, *126*, 3762.

(107) Glasoe, P. K.; Long, F. A. *Journal of Physical Chemistry* **1960**, *64*, 188.

(108) Das, D.; Dutta, T.; Nath, K.; Kotay, S. M.; Das, A. K.; Veziroglu, T. N. *Current Science* **2006**, *90*, 1627.

(109) Stewart, A. I.; Wright, J. A.; Greetham, G. M.; Kaziannis, S.; Santabarbara, S.; Towrie, M.; Parker, A. W.; Pickett, C. J.; Hunt, N. T. *Inorganic Chemistry* **2010**, *49*, 9563.

(110) Kaziannis, S.; Santabarbara, S.; Wright, J. A.; Greetham, G. M.; Towrie, M.; Parker, A. W.; Pickett, C. J.; Hunt, N. T. *Journal of Physical Chemistry B* **2010**, *114*, 15370.

(111) Baiz, C. R.; McRobbie, P. L.; Anna, J. M.; Geva, E.; Kubarych, K. J. *Accounts of Chemical Research* **2009**, *42*, 1395.

(112) Roseboom, W.; De Lacey, A. L.; Fernandez, V. M.; Hatchikian, E. C.; Albracht, S. P. J. *Journal of Biological Inorganic Chemistry* **2006**, *11*, 102.